CAL
2)
15(2

気象庁欧文海洋報告

JUL 14 1964
FISH & WILDLIFE SERVICE

第15巻 第2号

THE OCEANOGRAPHICAL MAGAZINE

Vol. 15 No. 2

CONTENTS

Y. SUGIURA: Time and space variation of the T-Cl relation in Tokyo Bay... 67

M. YASUI, T. UMEZAKI and S. SATO: Short note on the operational breadth of level-winders of hydrographical winches..... 81

T. SAWARA: A short note on nomography for unprotected reversing thermometer..... 85

T. NAKAI: An attampt of slope corrections on echogram in deep-sea 89

T. UENO: Theoretical studies on tidal waves travelling over the rotating globe (I) 99

T. NAN'NITI, H. AKAMATSU, T. NAKAI and K. FUJII: An observation of a deep current in the southern east sea of Tori shima.....113

H. AKAMATSU: Preliminary report of the Japanese Expedition of Deep-Sea, the sixth cruise, 1963 (JEDS-6) 123

Published by the Japan Meteorological Agency

January 1964

The Oceanographical Magazine
Vol. 15. No. 2, January 1964

Time and Space Variation of the T-Cl Relation in Tokyo Bay

By

Yoshio SUGIURA

Meteorological Research Institute

(Received November 8, 1963)

Abstract: The T-Cl diagram for waters of Tokyo Bay was surveyed for obtaining some idea on the kinetic behaviour of the bay water, which should be the back-ground material for protection or prediction of water pollution hazard particularly due to the recent, highly probable radioactive contamination. The difference in distribution pattern of temperature and chlorinity between the surface and the bottom layer was pointed out. The exchange rate of waters between inside and outside the bay was estimated respectively for winter and summer season.

1. *Introduction*

Around the region including Tokyo Bay and Uraga Channel there are many sources of water pollution due to industrial, and living, wastes. In addition, a new source derived from radioactive wastes will be possibly put in place in near future. In considering protection or prediction of water pollution hazard, various aspects i.e. physical, chemical and biological should be taken into account. One of these aspects is the kinetic behaviour such as the exchange rate of bay water and oceanic water, current, diffusion rate and so on. Several publications are now available concerning temperature and chlorinity of Tokyo Bay and Uraga Channel. Then, the author intends to put these data in order for obaining some idea on the kinetic behaviour of the bay water. The data employed here is those obtained by the Tokai Regional Fisheries Research Institute. (1949).

2. *Seasonal variation in temperature and chlorinity*

Fig. 1 shows a T-Cl diagram in the Tokyo Bay and Uraga Channel region. The following conclusion can be drawn from Fig. 1:

(1) The Uraga Channel water near the entrance of Tokyo Bay maintains chlo-

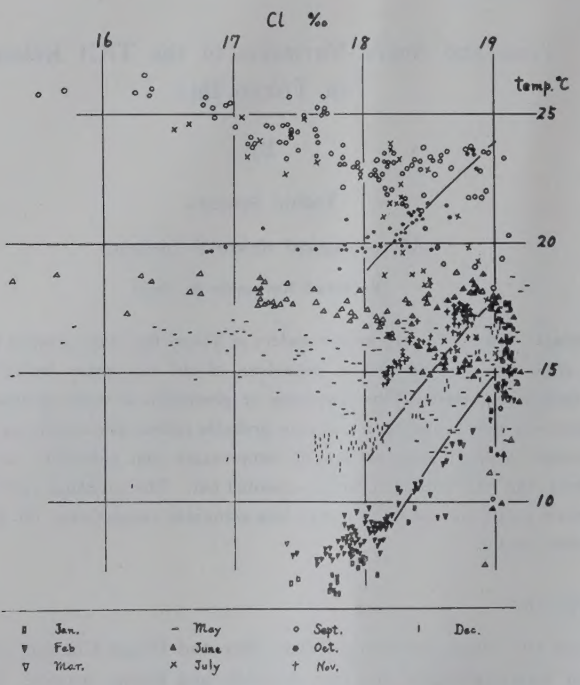

Fig. 1. A T-Cl diagram of Tokyo Bay in all seasons of the year

rinity of 19.0‰ throughout the year.

(2) On the other hand, the chlorinity of the water located at the deep end of Tokyo Bay is often less than 16‰. Particularly so in June and September, which suggests more abundant supply of fresh water by rain and run-off in those occasions.

(3) A periodical change can be seen in the T-Cl diagram, which is mainly due to the seasonal variation in temperature of river waters pouring into the bay. Temperature of sea water seasonally changes with some time-lag as compared to that of river water. (Concerning the seasonal variation of river waters, see NISHIZAWA's paper (1962)).

(4) During May to September there exists a remarkable difference in density between waters at surface and bottom. But during October to March only a slight difference exists and nearly all points in the T-Cl diagram stand on a certain isopycnal.

(5) During May to September some of the whole points representing temperature and chlorinity of waters observed in the two succesive months coincide. But during October to January no coincidence was found anywhere among them.

3. *The T-Cl diagram in May*

A T-Cl diagram in May is shown in Fig. 2. It takes a figure of an inverted triangle with one of apexes downward. Three apexes of this triangle represent three kinds of source waters. One of those apexes represents a property of the coastal water influenced to the uppermost degree by river water and another,

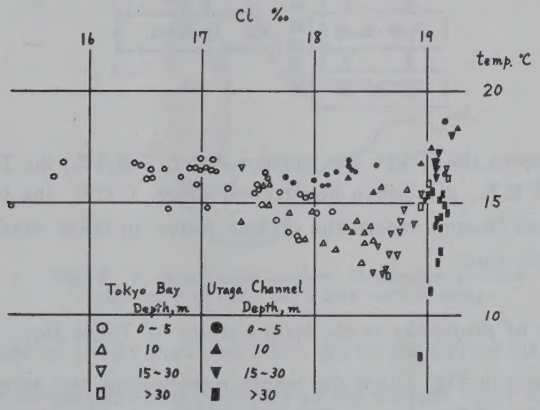

Fig. 2. A T-Cl diagram of Tokyo Bay in May

one of oceanic water, that is the Sagami Bay water in this case. The last one equivalent to the water of Cl 18.5‰ and t 12.5°C, which corresponds to the water mass located at the 15 m or deeper depth in Tokyo Bay. This water mass is, as pointed out previously, recognized to be in common with each other in the two, consecutive months, for example in April and in May. Therefore, it can be deduced that this water mass is the remaining portion of the water which occupied the Tokyo Bay bottom layers in the previous month.

Besides, Fig. 2 shows the following points:

(1) A mass of points extending to the left-hand side of the left apex of the triangle represent the water of the 0 to 5 m depth layer of Tokyo Bay. This and the water of the 15 m or deeper depth equivalent to the Tokyo Bay bottom water constitute the water of the 10 m depth through mutual mixing.

(2) The water of the 15 m or deeper depth is composed of the water of the Tokyo Bay bottom water (Cl 18.5‰ and t 12.5°C) and the Uraga Channel water of the 15 m or deeper depth at their various mixing ratio. The latter can not be distinguished from the Sagami Bay water. The Uraga Channel water of the 0 to 10 m depth is composed of the Tokyo Bay water and the Sagami Bay water at their various mixing ratio.

(3) The mentioned relation can be expressed schematically as follows:

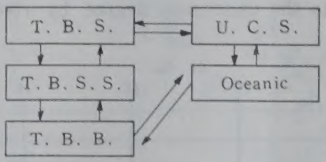

where T.B.S. means the Tokyo Bay surface water, T.B.S.S., the Tokyo Bay sub-surface water, T.B.B., the Tokyo Bay bottom water, U.C.S., the Uraga Channel surface water and Oceanic means the oceanic water, in other words, the Sagami Bay water in this case.

4. Distribution of properties in the bottom water of Tokyo Bay

It can be seen in Fig. 2 that the points representing the properties of the Tokyo Bay water of the 15 m or deeper depth lie on one side of peripheries of the triangle and the line was nearly parallel to the isopycnal. One of two apexes on this line is the point of Cl 18.5‰ and t 12.5°C and another is one of Cl 19.1‰ and t 17.0°C representing the Sagami Bay water. Points located between the two apexes along this line represent the properties of the water obtained through mixing of the Sagami Bay water and the bottom water of Tokyo Bay.

To express the degree of mixing along this line, the intercept between the two extremities was divided arbitrarily into six divisions, and the horizontal distribution of these six water types was shown in Fig. 3. According to Fig. 3, the one extremity is located at the deep end of the bay and another at the entrance of the bay. This distribution pattern is significantly different from that in the surface layer of the Tokyo Bay water which will be described later. This pattern suggests that the Tokyo Bay bottom water gradually exchanges with the Uraga Channel water and ultimately with the oceanic water through diffusion.

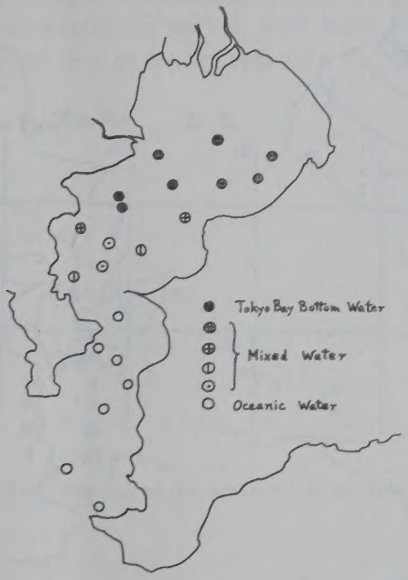

Fig. 3. A distribution pattern of temperature and chlorinity in the Tokyo Bay bottom layer.

5. Distribution of temperature and chlorinity in the surface water of Tokyo Bay

So far as temperature and chlorinity of the surface water are concerned, the eastern half of Tokyo Bay may be distinguished from the western half as shown in Fig. 4 to Fig. 6. It is higher in density at the eastern half. In other words, the western half is influenced to more extent by inland water. This trend suggests that there exists a stationary current running counter-clockwise inside the bay, because the main sources of the river water supply located at the deep end of the bay can give the mentioned distribution if the counter-clockwise current is assumed. While, at the 0 m depth sometimes the lighter water intrudes into the eastern half as shown in Fig. 7. Possibly this is ascribed to the capricious perturbation of the stationary current at the extreme surface by a strong wind and/or profuse run-off. Anyway, in the surface water the distribution pattern of temperature and chlorinity is quite different from that in the case of the bottom water. Directly above the bottom the current is weakened by the frictional resistence of the bottom, in the sequence of which the pattern as shown in Fig. 3 can be thought to be given.

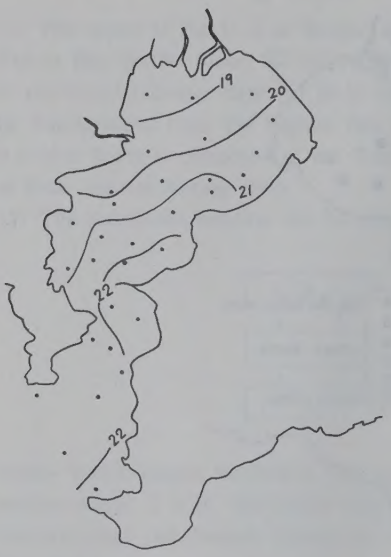

Fig. 4. σ_t distribution at 0 m depth, Sept., 1947.

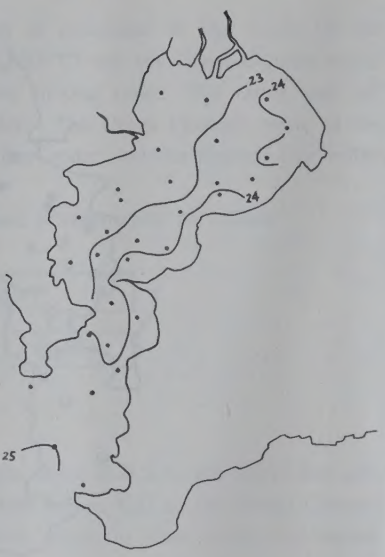

Fig. 5. σ_t distribution at 5 m depth, May, 1947.

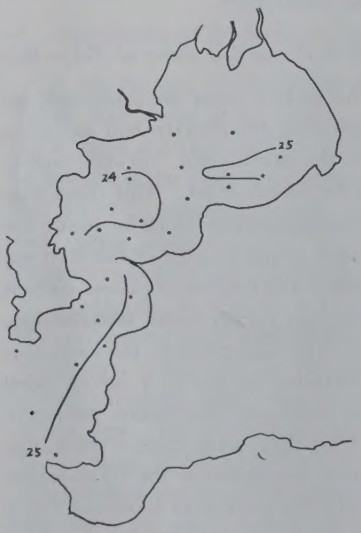

Fig. 6. σ_t distribution at 10 m depth, May, 1947.

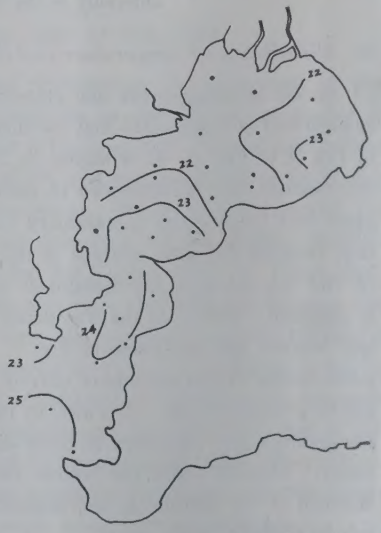

Fig. 7. σ_t distribution at 0 m depth, May, 1947.

Fig. 8 shows the T-Cl diagram pertaining to the western half of Tokyo Bay, in which a mass of points representing the 0 m depth water occupy the left-hand side, those representing the 15 m or deeper depth water the right and those repre-

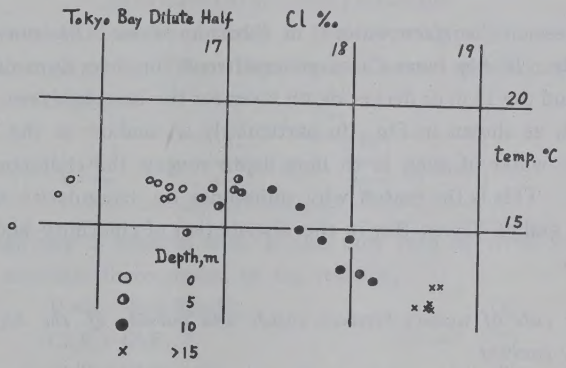

Fig. 8. A T-Cl diagram of the western half of Tokyo Bay.

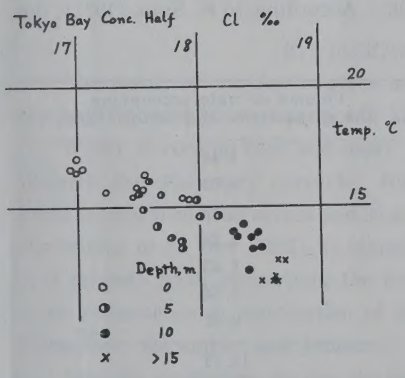

Fig. 9. A T-Cl diagram of the eastern half of Tokyo Bay.

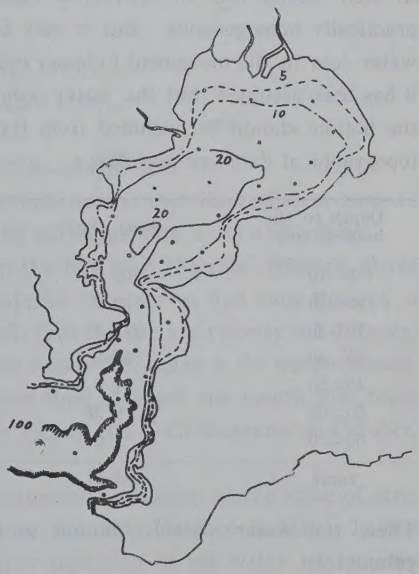

Fig. 10. Bottom topography of Tokyo Bay. Figures express depth in meter.

senting the 10 m depth water the middle. Fig. 9 shows the T-Cl diagram pertaining to the eastern half. The same thing can be said also in this case, but the chlorinity corresponding to each layer in the eastern half is higher than in the western half.

The expression "surface water" or "bottom water" has not hitherto been used so strictly. It only means as a general trend the 0 to 10 m depth layer for the surface and the 15 m or deeper depth layer for the bottom layer. But actually, Tokyo Bay is, as shown in Fig. 10, particularly so shallow at the north-eastern end that the water of even 12 to 15 m depth reveals the characteristics as the bottom water. This is the reason why sometimes the irregularity appears at the north-eastern end of Tokyo Bay in the distribution of chlorinity and temperature at each depth.

6. *Exchange rate of waters between inside and outside of the bay due to the stationary current*

Firstly, the winter season will be considered. In winter water is vertically so well mixed due to convection that the vertical distribution of properties is practically homogeneous. But it may be supposed that some part of the bottom water join in the movement to lesser extent. Accordingly, only for the simplicity it has been assumed that the water occupying the layer 5 m thick directly above the bottom should be excluded from the bulk. According to K. SUDA (1931), the topographical data are as follows:

Depth to the bottom (m)	Area (km^2)	Volume of water occupying the space above the bottom (km^3)
5—10	192.0	1.44
10—20	328.3	4.92
20—30	211.5	5.29
30—40	63.5	2.22
40—50	31.7	1.43
50—60	6.25	0.34
60—70	1.0	0.07
total	834.2	15.71

Then, the water actively joining in the mentioned movement occupies the volume of

$$15.71\ km^3 - 834.2\ (5/1000)\ km^3 = 10.54\ km^3.$$

According to the observation made in December on the three main rivers pouring

into the bay (See the publication issued from the Japan Electric Agency), i.e. Tama, Ara and Edo river, the total flow rate is 1×10^7 m^3/day. Then, the exchange rate will be

$$10.54\times10^9/(30.8)\,(1\times10^7)=34 \text{ days.}$$

Here the figure of 30.8 can be obtained in the following way:

Water exchange among Tokyo Bay, Uraga Channel and Sagami Bay can be expressed schematically as

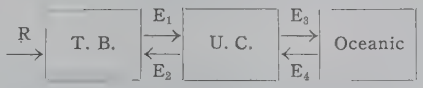

where exchange rate is denoted with E and flow rate of river water with R. Among these amounts there should be the relation,

$$R=E_1-E_2=E_3-E_4, \quad (1)$$

$$Cl_uE_2=Cl_tE_1, \quad (2)$$

$$Cl_uE_3=Cl_oE_4, \quad (3)$$

where Cl_o, Cl_u and Cl_t show chlorinity of the oceanic, Uraga Channel and Tokyo Bay water respectively.

Solving these formulae,

$$E_1=Cl_uR/(Cl_u-Cl_t)$$

can be obtained, where $Cl_u=18.5‰$ and $Cl_t=17.9‰$.

So,

$$E_1=18.5R/(18.5\text{-}17.9)=(30.8)\ R.$$

The result of calculation gives us the information that the turn-over time of the bay water is about one month and the exchange rate is 3.1×10^8 m^3/day.

Water is coming into and away from the bay with the rate obtained above through the stationary current. Now suppose the current flux runs through a cross section with 5 km across and 20 m thick, then the current velocity is 0.07 knots. Accordihg to K. Ono (1951), it ranges from 0.03 to 0.37 knots in the winter season. It is another proof concerning the turn-over time of about one month that there is no coincidence in distribution of points among the T–Cl diagrams of October, November, December and January.

Now let us discuss on the stationary current appearing at the state of stratification in the summer season by using the data obtained in May. In this season temperature of river water is higher than that of sea water in the bay and the bay water stratifies with an evident vertical gradient of density. There is no homogeneity covering the whole column of water unlike in the previous

case. Then, the simplified model as mentioned before can not be employed here.

The T-Cl diagram of May being taken into account, the model as shown in Fig. 11 can be employed. In Fig. 11 T. B. S. D. H denotes Tokyo Bay surface dilute half, T.B.S.C.H., Tokyo

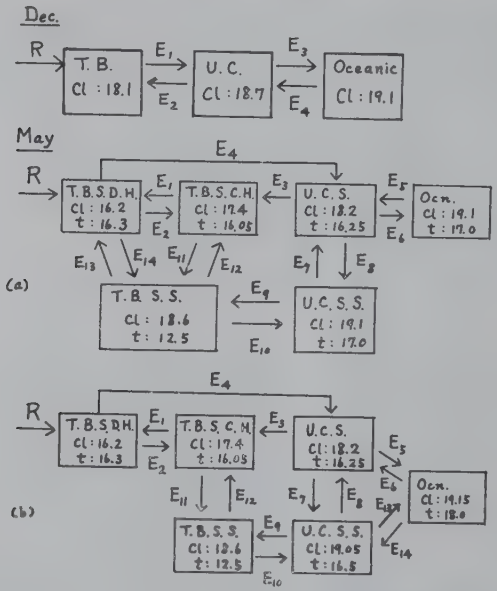

Fig. 11. Schematic model composed of several water types in Tokyo Bay.

Bay sub-surface, U.C.S., Uraga Channel surface, U.C.S.S., Uraga Channel sub-surface and O.S., oceanic surface. The following constants are respectively used for these water types.

Water type	Suffix to be used	Cl (‰)	t (°C)
T. B. S. D. H.	1	16. 2	16. 3
T. B. S. C. H.	2	17. 4	16. 05
T. B. S. S.	3	18. 6	12. 5
U. C. S.	4	18. 2	16. 25
U. C. S. S.	5	19. 1	17. 0
O. S.	6	19. 1	17. 0

The flow rate of river water is expressed with R and the exchange rate of water between water masses with E. Temperature of river water is expressed with t_r. It is assumed that exchange rate including flow rate, chlorinity and temperature are maintained constant with respect to each water mass. Then,

$$-E_1+E_2+E_4-E_{13}+E_{14}=R, \quad (1)$$
$$E_1-E_2-E_3+E_{11}-E_{12}=0, \quad (2)$$
$$E_3-E_4-E_5+E_6-E_7+E_8=0, \quad (3)$$
$$-E_5+E_6=R, \quad (4)$$
$$E_7-E_8+E_9-E_{10}=0, \quad (5)$$
$$Cl_2E_1-Cl_1E_2-Cl_1E_4+Cl_3E_{13}-Cl_1E_{14}=0, \quad (6)$$
$$Cl_2E_1-Cl_1E_2-Cl_4E_3+Cl_2E_{11}-Cl_3E_{12}=0, \quad (7)$$
$$Cl_6E_5-Cl_4E_6=0, \quad (8)$$
$$Cl_5E_7-Cl_4E_8+Cl_5E_9-Cl_3E_{10}=0, \quad (9)$$
$$Cl_5E_9-Cl_3E_{10}+Cl_2E_{11}-Cl_3E_{12}-Cl_3E_{13}+Cl_1E_{14}=0, \quad (10)$$
$$-t_2E_1+t_1E_2+t_1E_4-t_3E_{13}+t_1E_{14}=Rt_r, \quad (11)$$
$$t_2E_1-t_1E_2-t_4E_3+t_2E_{11}-t_3E_{12}=0, \quad (12)$$
$$t_4E_3-t_1E_4-t_6E_5+t_4E_6-t_5E_7+t_4E_8=0, \quad (13)$$
$$t_5E_7-t_4E_8+t_5E_9-t_3E_{10}=0, \quad (14)$$
$$-t_6E_5+t_4E_6+V\cdot\triangle t=Rt_r, \quad (15)$$

where V denotes the volume occupied by the Tokyo Bay bottom water (T.B.S.S.). And $\triangle t$ is the increment of water temperature for a unit time duration. Into these equations were introduced the constants shown above beside $R=208\ m^3/sec$ and $t_r=18.0°C$. As the result the following answers were obtained for the model (a) but no answer for the model (b) shown in Fig. 11.

E_1 3,019 m^3/sec,
E_2 -3,433,
E_3 -4,414,
E_4 -0.0016,
E_5 4,206,
E_6 4,414,
E_7 -4,206,
E_8 -0.002,
E_9 4,206,
E_{10} -0.0000,
E_{11} -11.357 m^3/sec,
E_{12} -490,
E_{13} -105,

E_{14} 6,555,

$V \cdot \triangle t$ 3,519 °C m³/sec.

The results obtained here require the re-construction of the block diagram as shown below.

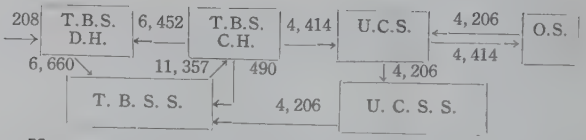

$V \cdot \triangle t = 3{,}519$

The results obtained above seem not to be entirely valid in the details, yet a general trend still can be well understood as shown below. That is, the results suggest the following points. There exists a stationary flow inside the bay, the flux of which is about 6,500 m³/sec. To this the flux of 4,200 m³/sec is added from the ouside of the bay, and moreover, the river water is added at the rate of 208 m³/sec. At the same time, water outflows at the rate of 4,400 m³/sec from the bay to the ocean through Uraga Channel. Therefore, now assuming that for the simplicity the Tokyo Bay water exchanges with the Uraga Channel water at the rate of 4,300 m³/sec, the turn-over time only due to a stationary current of the Tokyo Bay water in days is

$$10.5 \times 10^8 / 3.72 \times 10^4 = 28.2$$

where it is assumed that the water staying within 5 m above the bottom does not follow the stationary flow.

Now, about the validity of $V \cdot \triangle t = 3{,}519$ °Cm³/sec, a few words will be added. When the observational results are compared between May and June, the value of 2.75°C is obtained as $\triangle t$. So, the value of 3.3 km³ can be obtained as V. It being taken into account that the bottom layer is confined within 5 m above the bottom, the area to be occupied by water of bottom layer is $3.3 \times 10^6 / 5$ m². That is 660 km². While, according to SUDA, the area of the region of 10 m or deeper depth is 640 km².

In conclusion, the turn-over time of the Tokyo Bay water following the stationary current seems to be about one month irrespective of seasons of the year, but the bottom water does not follow satisfactorily the stationary current and its turn-over time is somewhat different from the aforementioned time. The change in properties of the bottom water takes place due to not only lateral mixing but also vertical mixing. The change due to the vertical mixing of the

bottom layer is probably more prominent in the winter season when convection overwhelms than in the summer season when stratification takes place. This is the reason why some of points coincide with each other in the T-Cl diagrams of successive two months in the summer season, while there is no coincidence among the T-Cl diagrams of the winter season. In other words, the change in properties of the botton water due to mixing can be considered to take longer time than one month in summer season.

The author was asked by Prof. Y. MIYAKE, Tokyo Kyoiku University and the Geochemical Laboratory, Meteorological Research Institute to take a glimpse of the oceanographical condition in Tokyo Bay in relation to the problem regarding the radioactive contamination. Thereafter the study was started The author wishes to express his hearty thanks to Prof. MIYAKE for having given him a chance of study.

References

Japan Electric Agency (1930): Abstracts of flow amounts of rivers. No. 2, pp. 449. (in Japanese).

NISHIZAWA, T. (1962): Temperature of river waters. Suion no Kenkyu (Study of Water Temperature), **6**, (2-7), 116-117, 149-155, 194-196. (in Japanese).

ONO, K. (1951): Tidal current in Tokyo Bay. Suiro-yoho, **25**, 245-253. (in Japanese).

SUDA, K. (1931): Report on the oceanographical survey of Tokyo Boy. Kaiyo-jiho, **3**, 1-119. (in Japanese).

The Oceanographical Magazine
Vol. 15. No. 2, January 1964

Short Note on the Operational Breadth of Level-Winders of Hydrographical Winches

By

Masashi YASUI *Maizuru Marine Observatory*
Takashi UMEZAKI *Toyo Electric Manufacturing Co., Ltd.*
Saburo SATO *Tamagawa Industrial Co., Ltd.*

(Received November 27, 1963)

Hydrographical winches carry large amounts of wire rope. To lay the wire smoothly on drums without uneven accumulation, level-winders or spreaders of some types are necessary. So far, many types, which are mechanically and automatically driven, have been designed and utilized. However, the relationship between the inner breadth of drums and the operational breadth of levelwinders have not completely settled. The relationship is an important part of the designe: If the operational breadth of level-winders is too large, the packing of the wire will break the flanges away accumulating in the end-parts of the drum: If too small, the wire will be severely damaged when overlying coils slip down into a gap between the packed coil and the flanges. It is desirable to lay wire on the drum so as to have room for one turn of the wire rope or less between the packed coil and the flanges. The operational breadth of levelwinders do not coincide with the actual breadth of packed coil on the drum. The authors would like to present an approximate relation between them.

Let us denote the distance between the axes of drums and level-winders as l, the diameter of a trunk of drums as R, the rotational speed of drums as n, the speed of level-winders as v, and the incident angle of the wire to drums as θ at a certain time. After an infinitesimal small time dt, the relation will be as follows;

$$l\tan\theta - vdt - \pi Rndt\tan\theta = l\tan(\theta+d\theta), \qquad (1)$$

where $d\theta$ is the amount of change in θ during dt. When the amount of θ is so small that $\tan\theta$ and $\tan(\theta+d\theta)$ can be replaced by θ and $\theta+d\theta$, we obtain the following differential equation from (1);

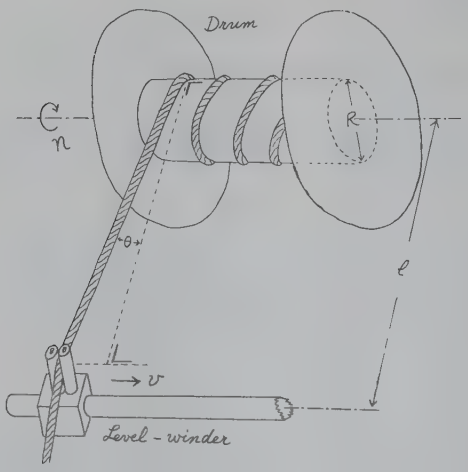

Fig. 1.

$$d\theta/dt=-\frac{v+\pi Rn\theta}{l}. \tag{2}$$

Integrating this equation, the next relation follows;

$$\theta=Ce^{-\frac{\pi Rn}{l}t}-\frac{v}{\pi Rn}. \tag{3}$$

For the initial condition, we assume that the angle θ is θ_0 at the time $t=0$. Then,

$$C=\theta_0+\frac{v}{\pi Rn}. \tag{4}$$

However, the amount of θ must tend to $-v/\pi Rn$ after a long time. In this system, it is reasonable to assume that $|\theta|=v/\pi Rn$ when the level-winders turns over at the extreme points. When the initial time $t=0$ is taken to coincide with the time of turning, integration constant (4) is reduced as follows;

$$C=\frac{2v}{\pi Rn}.$$

Then the solution (3) is

$$\theta=\frac{2v}{\pi Rn}e^{-\frac{\pi Rn}{l}t}-\frac{v}{\pi Rn}. \tag{5}$$

From this, the time at which the angle θ is reduced to zero is obtained as follows;

$$t_0=\frac{l}{\pi Rn}\log_e 2.$$

During the time, the level-winder travels inwards as far as vt_0. In other words, the operational breadth of level-winders has to be vt_0 wider in both ends than the breadth of the packed coil on the drum. Now, we denote this vt_0 as Δb, and the breadth of packed coil on the drum as b. Then Δb is represented by

$$\Delta b = \frac{lv}{\pi Rn} \log_e 2 \simeq 0.2207 \frac{lv}{Rn}. \qquad (6)$$

Introducing the movement p of level-winder per one rotation of the drum or the number N of rotations of the drum per a double-trip of level-winders, v/n is reduced to p or $2\frac{b+2\Delta b}{N}$. Substituting these into (6), we obtain the following;

$$\Delta b = 0.2207 \frac{lp}{R} = \frac{0.441lb/NR}{1-0.883l/NR}.$$

The Oceanographical Magazine
Vol. 15. No. 2, January 1964

A Short Note on Nomography for Unprotected Reversing Thermometer

By

Tsutomu SAWARA

Japan Meteorological Agency

(Received Dec. 25, 1963)

The depth of reversal of unprotected thermometers D is calculated from the well-known formula (e.g. SVERDRUP et. al., 1949)

$$D=10\frac{T_p-T_w}{k\bar{\rho}},$$

where T_p and T_w are the corrected readings of unprotected and protected revers-

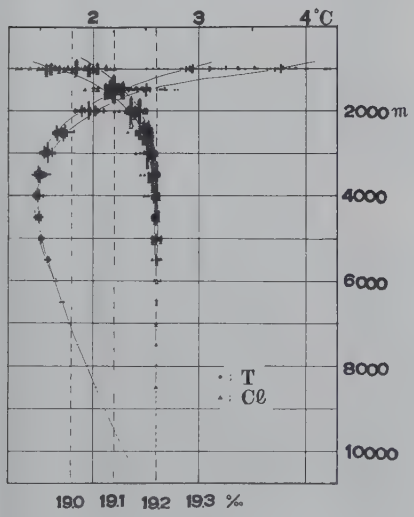

Fig. 1. Synthetic distribution of temperature and chlorinity in deep-seas adjacent to Japan.

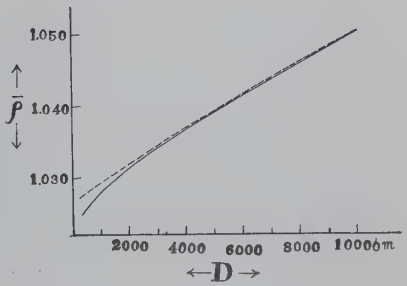

Fig. 2. Relationship between mean density and depth in deep-seas adjacent to Japan.
—— in Kuroshio water
..... in Oyashio water

ing thermometers respectively, $\bar{\rho}$ is the mean density *in situ* of the overlying water, and k, the pressure constant for the individual thermometer. For routine work within any limited area, it is convenient to establish a relationship between depth and mean density. We are used to adopt the relationship established by SUDA (1931) in the upper several thousands meters layers within the seas adjacent to Japan. However, it seems to need some correction for the relationship in the case of such a deep-sea hydrographical casts as of 10,000 m depth.

Results of the recent deep-sea hydrographical casts (MASUZAWA et. al., 1960, 1961, 1962) are sumarized in Fig. 1. From Fig. 2, we obtain a relationship between depth and mean density in Kuroshio and Oyashio waters. In the case, we adopted the following typical values in the upper 1,000 m layer; 27.0°C, 19.30 Cl‰ at the surface, 13.0°C, 19.10 Cl ‰ at the 500 m depth in Kuroshio; 0.0°C, 18.00 Cl ‰ at the surface, 2.2°C, 18.70 Cl ‰ at the 500 m in Oyashio.

Difference between mean densities in Oyashio and Kuroshio is so small that difference between results of calculations by mean densities in Kuroshio and Oyashio for the same value of $(T_p - T_w)$ seems to be less than observational errors.

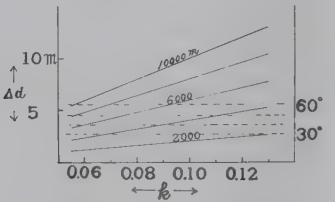

Fig. 3. Changes in depth when change of mean density is 0.001.
..... the greatest graduation of measurable range

Fig. 3 shows changes in calculated depth (Δd) for various values of k and various depth D, assuming 0.001 for the variation in the mean density. Therefore, it is quite reasonable to establish the unique relationship between the depth and the mean density for the purpose. Table 1 is calculated on the basis of the unique relationship, which is shown in the column of the extreme right.

Though the Table can be utilized for the depth determination, it is more convenient to introduce the following NAKAI's formula (Handbook for Marine Researcher, 1955);

$$D = \alpha(T_p - T_w) + \Delta D$$

For the simplicity of calculation, we think it is convenient if we adopt 100 for the value of α. Then, the value of ΔD can be briefly derived from Table 1.
Fig. 4 shows a part of the nomograph, by which we can obtain the value of ΔD

Table 1. Value of $(T_p - T_w)$ for different values of D and k.

$D\,(m)$ \ k	0.1280	0.1250	0.1200	0.1150	0.1100	0.1050	0.1000	0.0950	0.0900	0.0850	0.0800	0.0750	0.0700	0.0650	0.0600	D	ρ
500	6.570	6.416	6.160	5.903	5.646	5.390	5.133	4.876	4.620	4.363	4.106					500	1.0266
1000	13.166	12.858	12.343	11.829	11.315	10.800	10.286	9.772	9.257	8.743	8.229	7.714	7.200			1000	286
1500	19.780	19.316	18.544	17.771	16.998	16.226	15.453	14.681	13.908	13.135	12.362	11.590	10.818			1500	302
2000	26.409	25.790	24.758	23.727	22.695	21.664	20.632	19.600	18.569	17.537	16.506	15.474	14.442	13.411	12.379	2000	316
2500	33.056	32.281	30.990	29.699	28.408	27.116	25.825	24.534	23.242	21.951	20.660	19.369	18.078	16.786	15.495	2500	330
3000	39.717	38.286	37.235	35.683	34.132	32.581	31.029	29.477	27.926	26.375	24.823	23.272	21.720	20.169	18.617	3000	343
3500						38.058	36.246	34.434	32.621	30.809	28.997	27.184	25.372	23.560	21.748	3500	356
4000						43.546	41.472	39.398	37.325	35.251	33.178	31.104	29.030	26.957	24.883	4000	368
4500							46.710	44.374	42.039	39.704	37.368	35.032	32.697	30.362	28.026	4500	380
5000							51.960	49.362	46.764	44.166	41.568	38.970	36.372	33.774	31.176	5000	392
5500								54.361	51.500	48.639	45.778	42.916	40.055	37.194	34.333	5500	1.0404
6000								59.371	56.246	53.122	49.997	46.872	43.747	40.622	37.498	6000	416
6500								64.386	60.998	57.610	54.220	50.831	47.443	44.054	40.665	6500	427
7000								69.413	65.759	62.106	58.453	54.800	51.146	47.493	43.840	7000	438
7500								74.456	70.538	66.619	62.700	58.781	54.862	50.944	47.025	7500	450
8000								79.504	75.319	71.134	66.950	62.766	58.582	54.397	50.213	8000	461
8500												66.759	62.308	57.858	53.407	8500	472
9000												70.760	66.043	61.326	56.608	9000	483
9500												74.770	69.785	64.800	59.816	9500	494
10000												78.788	73.535	68.282	63.030	10000	505
10500												82.814	77.293	71.772	66.251	10500	1.0516
11000													81.058	75.269	69.478	11000	527

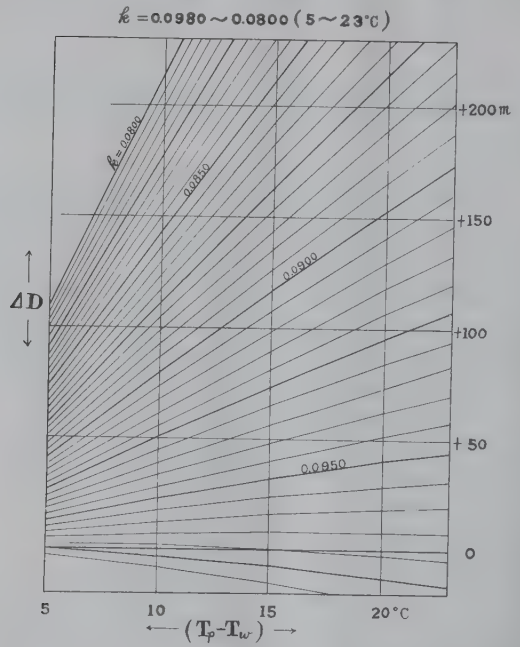

Fig. 4. A part of nomography, which shows the relationship between $(T_p - T_w)$, k and ΔD.

from the values of $(T_p - T_w)$ and k. The table and figure are very helpful to us not only for the calculation of thermometer reversing depth but also for the manufacturing of thermometers.

References

MASUZAWA, J., M. YASUI and H. AKAMATSU (1960): A hydrographic section across the Kurile Trench. *Oceanogr. Mag.* **11** (2), 1960.

MASUZAWA, J., M. YASUI and H. AKAMATSU (1961): Preliminary reports of the Japanese Expedition of Deep-Sea, the third cruise (JEDS-3). *Oceanogr. Mag.* **12** (2), 1961.

MASUZAWA, J., M. YASUI and H. AKAMATSU (1962): Preliminary reports of the Japanese Expedition of Deep-Sea, the fourth cruise (JEDS-4). *Oceanogr. Mag.* **13** (2), 1962.

SUDA, K (1931): On the exact determination of the depth of the observed layers by means of the non-protected reversing deep-sea thermometers. *Journal of Oceanography*, Imperial Marine Observatory, 2 (4), 1931. (in Japanese).

Handbook for the marine researcher, Japan Meteorological Agency. 1955. (in Japanese).

The Oceanographical Magazine
Vol. 15. No. 2, January 1964

An Attempt of Slope Corrections on Echogram in Deep-sea

By

Toshisuke NAKAI
Japan meteorological Agency

(Received Dec. 25, 1963)

Abstract: A new method of slope correction on the deep-sea echogram was presented. Since the echo-length depends upon the characteristics of beam of transducer and of bottom configurations, it is necessary to obtain some relationships between echo-length and inclination of the sea floor. Several practical nomographs for estimating the mean inclinations of the ocean floor from echo-length and some other nomographs for routine use are presented.

1. *Introduction*

Though echo sounder may be the most useful apparatus for the bathymetric study of the ocean floor, many corrections and precautions must be taken in the work. Among them, sound velocity correction and slope correction are well known. YASUI, the author and collaborator (1962) had already established a method of sound velocity correction which may applicable within seas adjacent to Japan.

The problem of slope correction have been discussed by many authors (e.g. FISHER, 1954; HERDMAN, 1955). Of cause, we could get correct values of soundings by means of a sort of an approach method provided soundings lines should be placed at very closed intervals. In practice, however, it is impossible to survey a vast ocean area with such fine mesh. SCHÜLER (1951) presented an interesting problem using lengths of echo.

Though some type of echosounders record the bottom topography by a single line, echo from the bottom is generally accompanied with some extension of signals.

The echo-length, time duration of the extension, depend on the character of beam of the transducer and of the bottom configurations.

In this paper, the author would like to present an attempt to bring the SCHÜLER's idea into routine work.

2. *Geometry of the echo-length*

Characters of the beam of the transducer are represented by the half-diminish

angle. Now, we assume that signals emitted from transmitter are of breadthless pulse and echo within the beam of half diminish angle can be recorded. Then we can obtain several relationships which must contribute to determination of more accurate depth. Notations in the section are summarized in the following:

α; half-diminish angle,
d; depth of starting point of echo-length,
d'; depth of final point of echo-length,
D; depth vertically below the ship,
r; radius of beam with half-diminish angle at sea floor,
θ; inclination of the sea floor.

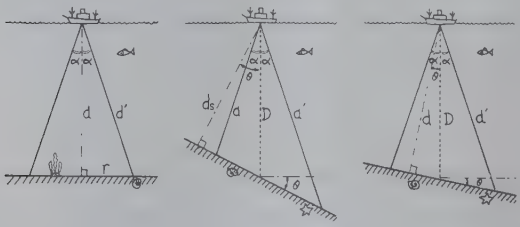

Fig. 1. (Left). Flat and horizontal floor.
Fig. 2. (Middle). Flat inclined floor ($\theta > \alpha$).
Fig. 3. (Right). Flat inclined floor ($\theta < \alpha$).

Case 1: Flat and horizontal floor. (Fig. 1)

Echo-length l is given by

$$l = d' - d = d\left(\frac{1}{\cos\alpha} - 1\right)$$

and

$$\gamma = d \tan\alpha.$$

Results of the computations are summarized in Fig 4.

Case 2: Flat inclined floor.

When $\theta > \alpha$, a line is drown from the ship's position perpendicular to the floor and let the length of the line denote ds as shown in Fig. 2. Then

$$d' = \frac{ds}{\cos(\theta+\alpha)} = d\frac{\cos(\theta-\alpha)}{\cos(\theta+\alpha)},$$

therefore, echo-length l is given by

$$l = d' - d = d\left\{\frac{\cos(\theta-\alpha)}{\cos(\theta+\alpha)} - 1\right\}. \qquad (1)$$

And the depth D vertically below the ship is given by

$$D=\frac{ds}{\cos\theta}=d\frac{\cos(\theta-\alpha)}{\cos\theta}. \qquad (2)$$

The correction for the reading of starting point of echo-length is as follows;

$$D-d=d\left\{\frac{\cos(\theta-\alpha)}{\cos\theta}-1\right\}.$$

When, $\theta>\alpha$, to the contrary, ds must be coincided with d, as shown in Fig. 3. Therefore, the following relations are obtained,

$$d'=\frac{d}{\cos(\theta+\alpha)},$$

$$l=d'-d=d\left\{\frac{1}{\cos(\theta+\alpha)}-1\right\}, \qquad (3)$$

$$D=\frac{1}{\cos\theta},$$

$$D-d=d\left\{\frac{1}{\cos\theta}-1\right\}. \qquad (4)$$

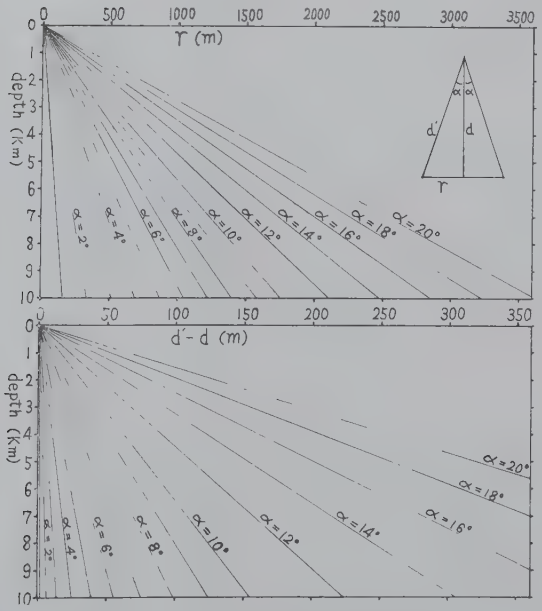

Fig. 4. Radius of beam with half-diminish angle and echo-length at horizontal floor.

The equations (1), (2), (3) and (4) are helpful to estimate the mean inclination of

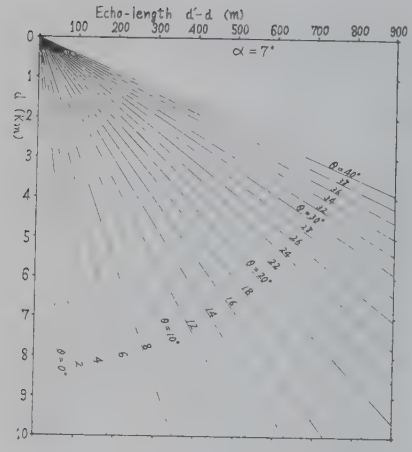

Fig. 5. Nomograph for estimating the mean inclination of the ocean floor from echo-length (α=7°).

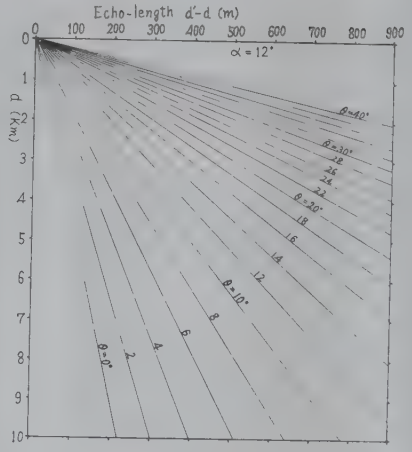

Fig. 6. Nomograph for estimating the mean inclination of the ocean floor from echo-length (α=12°).

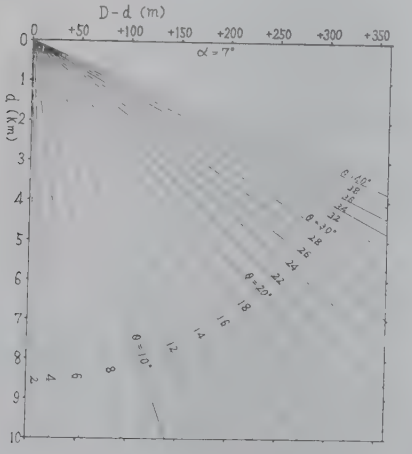

Fig. 7. Nomograph for estimating the conversion reading of starting point of echo-length to the depth vertically below the ship (α=7°).

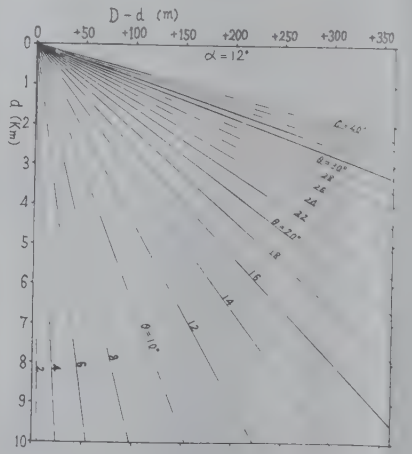

Fig. 8. Nomograph for estimating the conversion reading of starting point of echo-length to the depth vertically below the ship (α=12°).

the ocean floor within the beam and to convert the reading of starting point of echo-length to the depth vertically below the ship. As an example, the nomographs for the purpose are shown in Fig. 5 to 8, which are calculated $\alpha=7°$ and $12°$ respectively.

3. Manual for the routine work

The echo sounder generally has an attenuater with fine steps and continuous gain control. If not, it is necessary to attach the auxiliary apparatus of these types. Of cause, the attenuater has aleady to be calibrated.

The above stated geometry has been proceeded on the assumption that the breadth of emitted pulse-signal is instantaneously short. However, actual signals emitted from the transducer have a breadth of pulses though it is as short as 20 ms. The breadth of pulses depends upon not only the design of the sounder but also the adjustment of the machinery. The breadth can be determined by laboratory work, but it seems to be more practical to estimate by field work.

To calibrate the breadth of pulses, it is essential to let a vessel be at sea with fairly flat and horizontal bottom within the beam. The attenuater and gain control are properly regulated until we can obtain good records of echo sounding. After raising the attenuation by 12 db, the amplification is kept at a critical point just where records on sounder shall fade away, by adjusting the gain control. Fixing the gain control, the attenuation is restored to the former state. Thus, we are able to obtain the echo-length which is the sum of echo-lengths being due to the beam of half-diminish angle and the breadth of emitted pulses. The echo-length caused by the beam is able to be estimated from readings of the starting point of echo-lengths by the aid of Fig. 4. Difference between the echo-lengths recorded and calculated may be due to the breadth of pulses. It is desirable to do this calibration for the breadth of pulses whenever the vessel runs on seas with fairly flat and horizontal floor.

Even if the sounder records the bottom topography continuously, it is better to read the depth at certain interval, for instance, every 6 minutes or 10 minutes, and put down them on log sheets together with ship's position, course, speed and so on. Just before the reading, it is better to repeat the above procedure and to read the echo-length. Then we are able to estimate an inclination of sea floors and a depth vertically below the ship.

4. Directions of slopes

We can obtain the depth vertically below the ship and inclination of sea floor

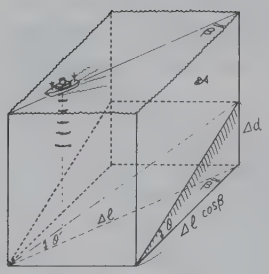

Fig. 9. The relationships among the deviation of ship's course, direction of slope, true and apparent inclination of bottom.

within the beam by the technique mentioned in the above section. On the other hand, we can obtain an apparent inclination of sea floors along the ship's course by records of echo-sounders and ship's speed. The difference between the mean and apparent inclinations depends on the discrepancy of the course from the direction of slopes.

The relationships between the deviations β of the ship's course from the direction of slopes, the true θ and apparent θ' inclinations are given by the following equation as shown in Fig. 9;

$$\tan\theta' = \cos\beta \tan\theta.$$

The relationship is summarized in Fig. 10,

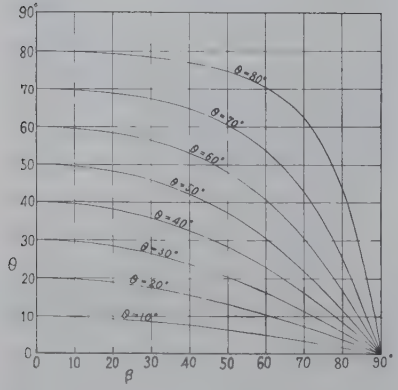

Fig. 10. Nomograph for estimating the direction of bottom slopes.

θ : inclination of the floor
θ': apparent inclination
β : deviation of the ship's course from the direction of slope

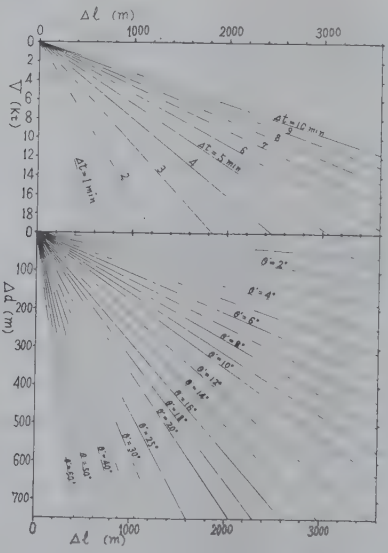

Fig. 11. Nomograph for estimating the apparent inclination along ship's course.

by which we can estimate the direction of bottom slopes. For the computation of the apparent inclination along ship's courses, the nomograph shown in Fig. 11 is convenient, which is deduced from

$$\tan\theta' = \frac{\Delta d}{\Delta t V} = \frac{\Delta d}{\Delta l},$$

where

θ'; apparent inclination,
Δd; depth differences during a certain time intervals Δt,
V; ship's speed,
Δl; run of the ship during a certain time interval Δt.

5. *Echograms for various types topographies*

The above stated discussion is proceeded under the assumption that the bottom is of plane. Actual topographies are sometimes so complicated that echogram recorded by sounders are not simple and monotonous. However, characteristic features of echograms are recorded for the peculiar topographies.

We notice echo from any one point **B** on the sea floor in Fig. 12. At the point $\boldsymbol{A}$ on the sea surface vertically over $\boldsymbol{B}$, the echogram of $\boldsymbol{B}$ shows us the true depth d.

At the surface point $\boldsymbol{A}_\theta$, where the angle between $\boldsymbol{A}_\theta\boldsymbol{B}$ and vertical is θ, the point $\boldsymbol{B}$ is recorded on the echogram as if $\boldsymbol{B}$ would be at $\boldsymbol{B}_\theta$ vertically bellow $\boldsymbol{A}_\theta$. The quantitative relationship between them are represented as follows;

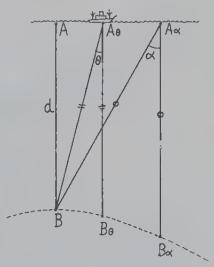

Fig. 12. Locus of echo from any one point.

$$\overline{\boldsymbol{A}_\theta\boldsymbol{B}_\theta} = \frac{d}{\cos\theta}, \qquad \overline{\boldsymbol{A}_\theta\boldsymbol{A}} = d\tan\theta.$$

Therefore,

$$\overline{\boldsymbol{A}_\theta\boldsymbol{B}_\theta}^2 - \overline{\boldsymbol{A}_\theta\boldsymbol{A}}^2 = d^2.$$

The last relation shows that the locus of $\boldsymbol{B}_\theta$ is a sheet of hyperboloid. Being θ is larger than the half diminish angle α, the echogram of $\boldsymbol{B}$ ought to be faded away.

By the aid of these relationships, we can geometrically construct echograms for any topography. Echograms for crossing various model structures are constructed in Fig. 13.

The actual bottom configurations are constructed with the combination of many sorts of structures. The echograms are not so simple as shown in Fig. 13.

However, studies of this sort give us useful mean for the interpretation. In Fig. 14, the echograms recorded on board of Ryōfū Maru and the interpretation of them are shown.

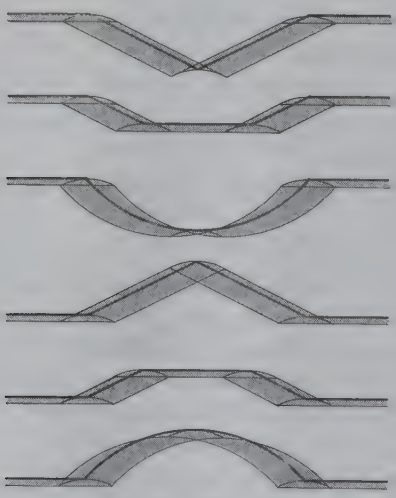

Fig. 13. Typical echograms for crossing various schematic bottom structures. Full lines indicate actual bottom.

Acknowledgement: The author wishes to express his thanks to Mr. M. YASUI, Maizuru Marine Observatory, who mentioned him the original idea, and Dr. M. HANZAWA, Japan Meteorological Agency, for his kind advices and encouragement.

References

YASUI, M., J. MASUZAWA, T. SAWARA and T. NAKAI (1961): Sounding of the Ramapo Deep. *Oceanogra. Mag.* **13** (1), 1961.

FISHER, R. L. (1954): On the sounding of trench. *Deep-Sea Research* **2** (1), 1954.

HERDMAN, H. F. P. (1955): Directional echo sounding. *Deep-Sea Research* **2** (4), 1955.

Schüler, F. (1951): Die Abbildungstreue von Meeresbonden-Profilen in Echogrammen. *Deutsche Hydrographische Zeitschrift* **4** (3), 1951.

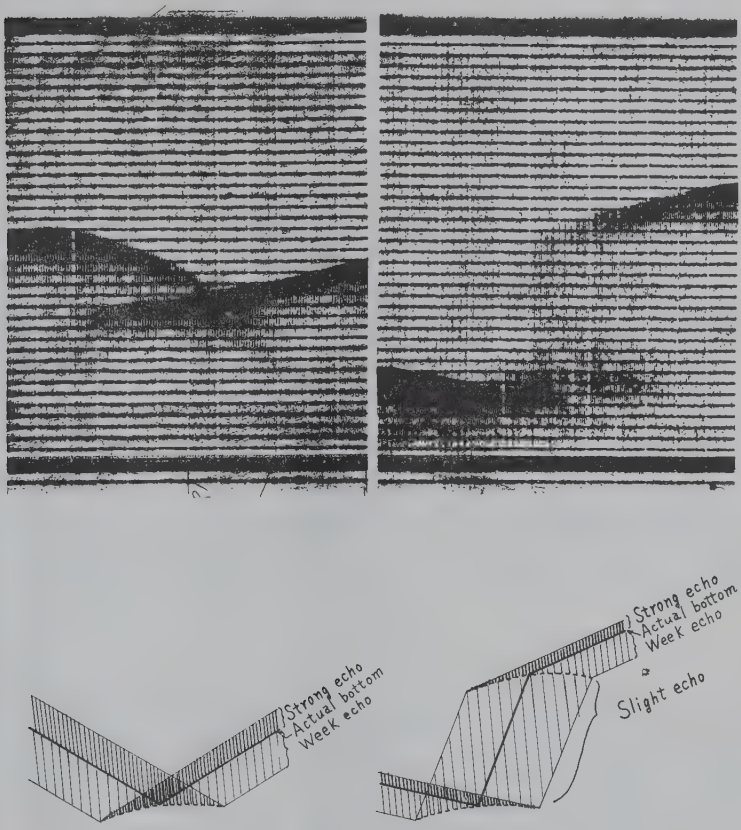

Fig. 14. The echograms recorded on board of the Ryōfū Maru, with the interpretation.

The Oceanographical Magazine
Vol. 15. No. 2, January 1964

Theoretical Studies on Tidal Waves Travelling over the Rotating Globe (I)

By

Takeo Ueno

Japan Meteorological Agency

(Received Dec. 23, 1963)

Abstract: Numerical Computations for tidal waves travelling over the oceans which cover the rotating globe were tried. Giving the tide-generating potential on the surface of the earth, the author numerically solved the hydrodynamical equations for the tides with the finite difference method. The bottom friction, the lateral mixing, the ellipticity of earth and the mutual attraction of the parts of the liquid were neglected. Considering the ability of the computer, the author divided the surface of the earth from the lat. 55°N to the lat. 75°S into the 5° meshes in direction of both long. and lat., with which the figure of continents, the depth of oceans are shown as correct as possible. At these grid points the tidal sea levels and the tidal currents were computed every 10 minutes time interval.

1. *Introduction*

The tides, the beautiful harmonic waves regularly surging upon without haste but without rest, have as much interested us as astronomy or mathematics since the origin of mankind. Therefore, for all ages and in all places, they are not only closely connected with our practical life but often famed in poetry, cited in proverb and appear in litterature. The history that the modern science has treated these phenomena is also quite long. Newton, Sir. I., Laplace, P. S., Poincaré, H. and other great scholars were much attracted in these miraculous phenomena and made efforts to solve the problem why and how the tides occur. Several means and theories to predict or explain the occurrence, amplitude or velocity of tides were reported by Kelvin,

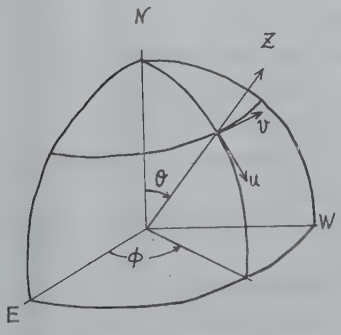

Fig. 1. The co-ordinate system.

L., DAWIN. G. H., HARRIS, R. A., AIRY, G. B., HOUGH, S. S., and other distinguished learned men. How to treat the tides and get the solution in hydrodynamics and methematics are admirably shown in detail in the wellknown "Hydrodynamics" by LAMB, H., and he seems to tell us that for all the difficulties to get the analytical solution for tides, it often gives us curious results which we can hardly understand comparing with the observations. This is, the author thinks, originated in so irregularity of the continents in figure and the oceans in depth that we cannot represent analytically the configuration of the sea covering the crust. Such the difficulties as seen in the other fields, however, have recently eliminated by the advent of highspeed automatic computers.

2. *The hydrodynamical equations for tides*

We adopt the coordinate system shown in Fig. 1. Then, the equations of motion and continuity for our problem are

$$\frac{\partial u}{\partial t}-2\omega v\cos\theta=-\frac{g}{a}\frac{\partial}{\partial\theta}(\zeta-\eta), \tag{1}$$

$$\frac{\partial v}{\partial t}+2\omega u\cos\theta=-\frac{g}{a\sin\theta}\frac{\partial}{\partial\phi}(\zeta-\eta), \tag{2}$$

$$\frac{\partial\zeta}{\partial t}=-\frac{1}{a\sin\theta}\left\{\frac{\partial}{\partial\theta}(hu\sin\theta)+\frac{\partial}{\partial\phi}(hv)\right\}, \tag{3}$$

where

θ : the co-latitude (the angle which the normal at any point on the undisturbed surface makes with the polar axis),

ϕ : the longitude measured eastwards,

z : the altitude measured outwards along the normal,

a : the radius of globe,

h : the depth of the sea asumed small with a, but not uniform,

g : the gravity at the surface neglected its variation with z and θ,

ω : the angular velocity of the earth,

u : the component velocity of the fluid along the meridian in the direction θ increasing,

v : the component velocity of the fluid along the latitude in the direction of ϕ increasing,

ζ : the elevation of the disturbed surface above the undisturbed level measured along z,

η : the statistic elevation of the sea corresponding to the potential of tide-

generating potential Ω, that is, $\eta=\Omega/g$.

Here, the bottom friction, lateral mixing, ellipticity of earth and the mutual attraction of the parts of the liquid are neglected. Further, the horizontal motion is assumed the same at all points in a vertical line. These hypotheses are not to sacrifice essential features for our problem in the case of treating the general motions of such the long wave in large scale on the actual earth.

3. *The potential of tide-generating force*

For the most important tide, the lunar semi-diurnal tide M_2, the statistic sea elevation corresponding to the potential are given by the following formula:

$$\eta_m(\theta,\phi,t)=\frac{3}{2}\frac{M}{E}\left(\frac{a}{c}\right)^3 a\left(\frac{1}{2}-\frac{5}{4}e^2\right)\cos^2\frac{I}{2}\sin^2\theta\cos(2T+2h-2s+2\xi-2\nu). \tag{4}$$

For the lunar diurnal tide O_1,

$$\eta_o(\theta,\phi,t)=\frac{3}{2}\frac{M}{E}\left(\frac{a}{c}\right)^3 a\left(\frac{1}{2}-\frac{5}{4}e^2\right)\sin I\cos^2\frac{I}{2}\sin 2\theta\cos\left(T+h-2s+\frac{\pi}{2}+2\xi-\nu\right), \tag{5}$$

where

E : the mass of earth 5.966×10^{27} gr,
M: the mass of moon $E/81.45$,
a : the mean radius of earth 6.37123×10^8 cm,
c : the mean distance between the moon and earth 3.84403×10^{10} cm,
e : the mean eccentricity of moon's orbit 0.054900489,
I : the mean inclination of moon's orbit to the equator, having the value from 18.3° to 28.6° according to N which is the longitude of moon's ascending node with the 18.6 years period,
T: the hour angle of mean solar measured from the meridian at ϕ,
h : the mean longitude of sun,
s : the mean longitude of moon,
ξ : $\widehat{I\gamma'}$ as shown in Fig. 2,
ν : $\widehat{I\gamma}$ as shown in Fig. 2.

In Fig. 2,

Eγ**E**′ : the equator,
Sγ**S**′ : the sun's orbit,
LNL′ : the moon's orbit,

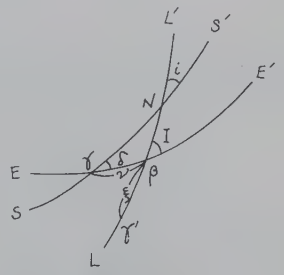

Fig. 2. The illustration of astronomical arguments.

γ : the vernal equinox,
$\mathbf{N}$: the moon's ascedning node,
$\widehat{\gamma\mathbf{N}}=\widehat{\gamma'\mathbf{N}}$.

4. The fundamental equations for the M_2 *tide*

In the formulas (4) we may write the argument as follows:

$$\left.\begin{aligned}\sigma_m t+2\phi&=2T+2h-2s\,,\\ \varepsilon_m&=2\xi-2\nu\,.\end{aligned}\right\} \tag{6}$$

Now, σ_m has the value 1.450 189 023$\times10^{-4}$ radian/sec, while ε_m varies with N having the so small range $\pm2.14°$ that we may neglect the variation. Further we put

$$H_m=\frac{3}{2}\frac{M}{E}\left(\frac{a}{c}\right)^3 a\left(\frac{1}{2}-\frac{5}{4}e^2\right)\cos^2\frac{I}{2}\,, \tag{7}$$

which has mean value 24 cm. Then the expressions for η_m, $\frac{\partial\eta_m}{\partial\theta}$ and $\frac{\partial\eta_m}{\partial\phi}$ become the following simple formula

$$\left.\begin{aligned}\eta_m(\theta,\phi,t)&=H_m\sin^2\theta\cos(\sigma_m t+2\phi)\,,\\ \frac{\partial\eta_m}{\partial\theta}&=2H_m\sin\theta\cos\theta\cos(\sigma_m t+2\phi)\,,\\ \frac{\partial\eta_m}{\partial\phi}&=-2H_m\sin^2\theta\sin(\sigma_m t+2\phi)\,.\end{aligned}\right\} \tag{8}$$

Let $F^\tau_{i,j}$ be the value of function $F(\theta,\phi,t)$ at any mesh point $\theta=i$, $\phi=j$ and time $t=\tau$,
and

$$M^\tau_{i,j}=h_{i,j}u^\tau_{i,j},\qquad N^\tau_{i,j}=h_{i,j}v^\tau_{i,j}\,, \tag{9}$$

$$S_i=\sin\theta_i\,,\qquad C_i=\cos\theta_i\,. \tag{10}$$

Then the differential equations (1), (2) and (3) will be rewritten with the finite difference method as follows:

First at $\theta=i$, $\phi=j$ and $t=\tau$ the equation (3) becomes

$$(\zeta^{\tau+1}_{i,j}-\zeta^{\tau-1}_{i,j})\frac{1}{\Delta t}=\frac{-1}{aS_i}\left[\frac{M^\tau_{i+1,j}S_{i+1}-M^\tau_{i-1,j}S_{i-1}}{\Delta\theta}+\frac{N^\tau_{i,j+1}-N^\tau_{i,j-1}}{\Delta\phi}\right],$$

$$\therefore\quad \zeta^{\tau+1}_{i,j}=\zeta^{\tau-1}_{i,j}$$

$$-\left[\frac{\Delta t}{a\Delta\theta}\frac{S_{i+1}}{S_i}M^\tau_{i+1,j}-\frac{\Delta t}{a\Delta\theta}\frac{S_{i-1}}{S_i}M^\tau_{i-1,j}+\frac{\Delta t}{a\Delta\phi}\frac{1}{S_i}N^\tau_{i,j+1}-\frac{\Delta t}{a\Delta\phi}\frac{1}{S_i}N^\tau_{i,j-1}\right]. \tag{11}$$

Next, at $\theta=l$, $\phi=k$ and $t=\tau+1$ the equation (1) becomes

$$\frac{M_{l,k}^{\tau+2}-M_{l,k}^{\tau}}{\Delta t}=2\omega C_l N_{l,k}^{\tau+1}-\frac{gh_{l,k}}{a}\frac{\zeta_{l+1,k}^{\tau+1}-\zeta_{l-1,k}^{\tau+1}}{\Delta\theta}+\frac{2H_m g h_{l,k}}{a}S_l C_l\cos(\delta_m t^{\tau+1}+2\phi_k),$$

$$\therefore\quad M_{l,\kappa}^{\tau+2}=M_{l,\kappa}^{\tau}+2\omega\Delta t C_l N_{l,\kappa}^{\tau+1}-\frac{g\Delta t}{a\Delta\theta}h_{l,\kappa}(\zeta_{l+1,\kappa}^{\tau+1}-\zeta_{l-1,\kappa}^{\tau+1})$$

$$+\frac{2H_m g\Delta t}{a}S_l C_l h_{l,\kappa}\cos(\sigma_m t^{\tau+1}+2\phi_k). \tag{12}$$

In the same way the equation (2) becomes

$$N_{l,\kappa}^{\tau+2}=N_{l,\kappa}^{\tau}-2\omega\Delta t C_l M_{l,\kappa}^{\tau+1}-\frac{g\Delta t}{a\Delta\phi}\frac{h_{l,\kappa}}{S_l}(\zeta_{l,\kappa+1}^{\tau+1}-\zeta_{l,\kappa-1}^{\tau+1})-\frac{2H_m g\Delta t}{a}S_l h_{l,\kappa}\sin(\sigma_m t^{\tau+1}+2\phi_k). \tag{13}$$

Now we put

$$\left.\begin{aligned}&\Delta\theta=\Delta\phi=\Delta\pi\ ,\\&X_{i+1,j}^{\tau}=\frac{\Delta t}{a\Delta\pi}S_{i+1}M_{i+1,j}^{\tau},\qquad Y_{i+1,j}^{\tau}=\frac{\Delta t}{a\Delta\pi}N_{i+1,j}^{\tau},\end{aligned}\right\} \tag{14}$$

the equation (11) takes the following simple formula

$$\zeta_{i,j}^{\tau+1}=\zeta_{i,j}^{\tau-1}-\frac{1}{S_i}[X_{i+1,j}^{\tau}-X_{i-1,j}^{\tau}+Y_{i,j+1}^{\tau}-Y_{i,j-1}^{\tau}]. \tag{15}$$

The equations (12) and (13) will become

$$X_{l,\kappa}^{\tau+2}=X_{l,\kappa}^{\tau}+2\omega\Delta t S_l C_l Y_{l,\kappa}^{\tau+1}-g\Big(\frac{\Delta t}{a\Delta\pi}\Big)^2 S_l h_{l,\kappa}(\zeta_{l+1,\kappa}^{\tau+1}-\zeta_{l-1,\kappa}^{\tau+1})$$

$$+2H_m g\frac{(\Delta t)^2}{a^2\Delta\pi}S_l^2 C_l h_{l,\kappa}\cos(\sigma_m t^{\tau+1}+2\phi_k), \tag{16}$$

$$Y_{l,\kappa}^{\tau+2}=Y_{l,\kappa}^{\tau}-2\omega\Delta t\frac{C_l}{S_l}X_{l,\kappa}^{\tau+1}-g\Big(\frac{\Delta t}{a\Delta\pi}\Big)^2\frac{1}{S_l}h_{l,\kappa}(\zeta_{l,\kappa+1}^{\tau+1}-\zeta_{l,\kappa-1}^{\tau+1})$$

$$-2H_m g\frac{(\Delta t)^2}{a^2\Delta\pi}S_l h_{l,\kappa}\sin(\sigma_m t^{\tau+1}+2\phi_k). \tag{17}$$

Now we provide that

$$X_{l,\kappa}^{\tau+1}=(X_{l,\kappa}^{\tau+2}+X_{l,\kappa}^{\tau})/2\ ,$$
$$Y_{l,\kappa}^{\tau+1}=(Y_{l,\kappa}^{\tau+2}+Y_{l,\kappa}^{\tau})/2\ ,$$

and put

$$\left.\begin{aligned}&A=2\omega\Delta t\ ,\\&B=g\Big(\frac{\Delta t}{a\Delta\pi}\Big)^2,\\&D=2H_m g\frac{(\Delta t)^2}{a^2\Delta\pi}\ ,\\&E=\frac{a\Delta\pi}{\Delta t}\ ,\end{aligned}\right\} \tag{18}$$

$$
\left.
\begin{aligned}
F1_l &= [1+A^2C_l^2/4]^{-1} \fallingdotseq 1\,,\\
F2_l &= [1-A^2C_l^2/4] \fallingdotseq 1\,,\\
F3_l &= AS_lC_l\,,\\
F4_l &= BS_l\,,\\
F5_l &= ABC_l/2\,,\\
F6_l &= DS_l^2C_l\,,\\
F7_l &= ADS_l^2C_l/2\,,\\
F8_l &= AC_l/S_l\,,\\
F9_l &= B/S_l\,,\\
F10_l &= ABC_l/2\,,\\
F11_l &= ADS_lC_l^2/2\,,\\
F12_l &= DS_l\,,\\
F13_l &= E/S_l\,,\\
F14_l &= E\,,\\
F15_l &= S_l\,.
\end{aligned}
\right\} \qquad (19)
$$

Then, our final form with which we compute the M_2 tide are

$$
\begin{aligned}
X_{l,\kappa}^{\tau+2} = X_{l,\kappa}^{\tau} + F3_l Y_{l,\kappa}^{\tau} - [F4_l(\zeta_{l+1,\kappa}^{\tau+1} - \zeta_{l-1,\kappa}^{\tau+1}) + F5_l(\zeta_{l,\kappa+1}^{\tau+1} - \zeta_{l,\kappa-1}^{\tau+1})\\
- F6_l\cos(\sigma_m t^{\tau+1} + 2\phi_\kappa) + F7_l\sin(\sigma_m t^{\tau+1} + 2\phi_\kappa)] \times h_{l,\kappa}\,, \qquad (20)
\end{aligned}
$$

$$
\begin{aligned}
Y_{l,\kappa}^{\tau+2} = Y_{l,\kappa}^{\tau} - F8_l X_{l,\kappa}^{\tau} - [-F10_l(\zeta_{l+1,\kappa}^{\tau+1} - \zeta_{l-1,\kappa}^{\tau+1}) + F9_l(\zeta_{l,\kappa+1}^{\tau+1} - \zeta_{l,\kappa-1}^{\tau+1})\\
+ F11_l\cos(\sigma_m t^{\tau+1} + 2\phi_\kappa) + F12_l\sin(\sigma_m t^{\tau+1} + 2\phi_\kappa)] \times h_{l,\kappa}\,, \qquad (21)
\end{aligned}
$$

$$
\zeta_{i,j}^{\tau+3} = \zeta_{i,j}^{\tau+1} - [X_{i+1,j}^{\tau+2} - X_{i-1,j}^{\tau+2} + Y_{i,j+1}^{\tau+2} - Y_{i,j-1}^{\tau+2}]/F15_t\,. \qquad (22)
$$

According to the formulas (20) and (21), if we put the initial values $X_{l,\kappa}^0$, $Y_{l,\kappa}^0$, $\zeta_{l\pm1,\kappa\pm1}^1$ are all null, we can compute the value $X_{l,\kappa}^2$ and $Y_{l,\kappa}^2$. Now that we know $\zeta_{i,j}^1$, $X_{l,\kappa}^2$ and $Y_{l,\kappa}^2$, using the formula (22) we can get $\zeta_{i,j}^3$, where mesh points (l, κ) and (i, j) are ajoining each other, the former is the point for the current and the latter the sea-level. Combining the formulas (20), (21) and (22), we get the current $(X_{l,\kappa}^{\tau+2}, Y_{l,\kappa}^{\tau+2})$ and the sea-elevation $\zeta_{i,j}^{\tau+3}$ alternatively with τ. The relations between (X, Y) and (u, v) are

$$
u_{l,\kappa}^{\tau} = F13_l X_{l,\kappa}^{\tau}/h_{l,\kappa}\,, \qquad (23)
$$

$$
v_{l,\kappa}^{\tau} = EY_{l,\kappa}^{\tau}/h_{l,\kappa}\,. \qquad (24)
$$

5. *The fundamental equations for the* O_1 *tide*

In the formula (5), the argument will be put as follows:

$$\left.\begin{aligned}&\sigma_0 t+\phi=T+h-2s\,,\\&\varepsilon_0=\frac{\pi}{2}+2\xi-\nu\,.\end{aligned}\right\}\tag{25}$$

The value of σ_0 is 0.6759774 radian/sec, while $2\xi-\nu$ varies with N having the so small rainge $\pm 10.94°$ that we may neglect the variation as in the case of σ_m. Further we put

$$H_0=\frac{3}{2}\frac{M}{E}\left(\frac{a}{c}\right)^3 a\left(\frac{1}{2}-\frac{5}{4}e^2\right)\sin I\cos^2\frac{I}{2}\,,\tag{26}$$

which has the mean value 10 cm. Then the expressions for η_0, $\frac{\partial\eta_0}{\partial\theta}$ and $\frac{\partial\eta_0}{\partial\phi}$ are

$$\left.\begin{aligned}&\eta_0(\theta,\phi,t)=H_0\sin 2\theta\cos\left(\sigma_0 t+\phi+\frac{\pi}{2}\right),\\&\frac{\partial\eta_0}{\partial\theta}=2H_0\cos 2\theta\cos\left(\sigma_0 t+\phi+\frac{\pi}{2}\right),\\&\frac{\partial\eta_0}{\partial\phi}=-H_0\sin 2\theta\sin\left(\sigma_0 t+\phi+\frac{\pi}{2}\right).\end{aligned}\right\}\tag{27}$$

In (19), if we put

$$\left.\begin{aligned}&F6_l=DS_l(C_l^2-S_l^2)\,,\\&F7_l=ADS_lC_l^2/2\,,\\&F11_l=ADC_l(C_l^2-S_l^2)/2\,,\\&F12_l=DC_l\,,\end{aligned}\right\}\tag{24}$$

we get the same fundamental equations for the O_1 tide computation as (20), (21) and (22) for M_2, with the different argument $\sigma_0 t+\phi+\frac{\pi}{2}$ instead of $\sigma_m t+2\phi$.

6. *Outline of computations*

Fig. 3 shows the computed area, where the earth's surface from the lat. 55°N to the lat. 75°S are divided into the 5° meshes, so in our program for the tidal computations $\Delta\pi=10°$. The excluded area is 10% to whole the sea surface, but the volume is only 5% to whole the ocean's volume.

The current velocity is computed at each grid point, where the depth is shown in 100 m unit. At all the grid points surrounded by four velocity points the elevations are computed, of which the dotted points numbered from one to 50 are the representative stations, where the elevations are tabled by the computer every time step which is $\Delta t=10$ min. in our case. The velocities and

elevations at all the grid points are mapped every hour. Those computed results and the co-tidal line will be shown in the next paper.

To campare our results with the observations is very interesting, but most tidal observations are affected from the continental shelves which causes the phase lag and the increasing of amplitude, while our model does not consider them. In the next paper we will show the comparison between our results at the representative stations and the observations at the corresponding isolated islands.

In the case of M_2 tide, we can easily get the tidal feature of the Atlantic Ocean in the "Oceans" by SVERDRUP, H. U. and others.

Fig. 4 shows the computed variations of elevations for M_2 at the representative stations in the Atlantic Ocean, where the numbers on each curve means the period of computation. According to these curves, in such the case as our model which begins the computations with the initial values all null, the computed values nearly converge after three periods. Fig. 5 and 6 are the comparisons of the amplitude (cm) and the phase lag (hour, G. S. T.) for M_2 between the results of third period mentioned above and the observations illustrated in the "Oceans". In Fig. 5, crosses indicate the observations, full lines by DEFANT, A. and dashed lines by author's computations. In Fig. 6 crosses indicate the observations, full lines by STERNECK, R. and dashed line by author's computations. (to be continued)

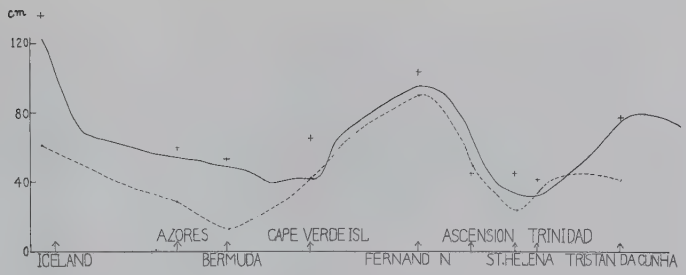

Fig. 5. The comparison of elevation (cm).
Crosses : Observations
Full lines : DEFANT, A
Dashed lines: Computed

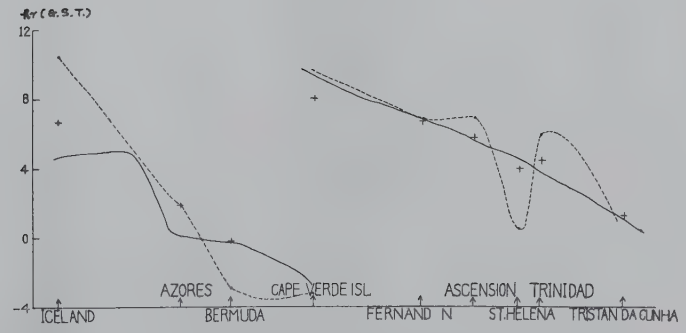

Fig. 6. The comparison of phase lag (G. S. T.)
Crosses : Observations
Full line : STERNECK, R
Dashed line: Computed

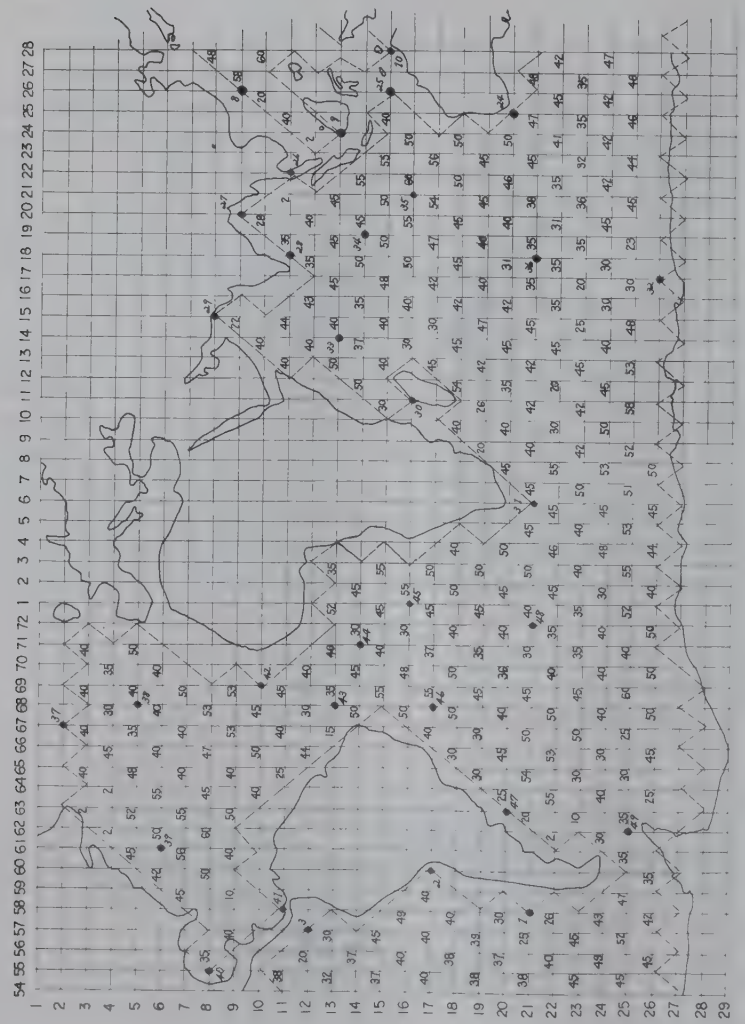

Fig. 3(a). Computed area and depth (100 m. unit). Dots are representative stations.

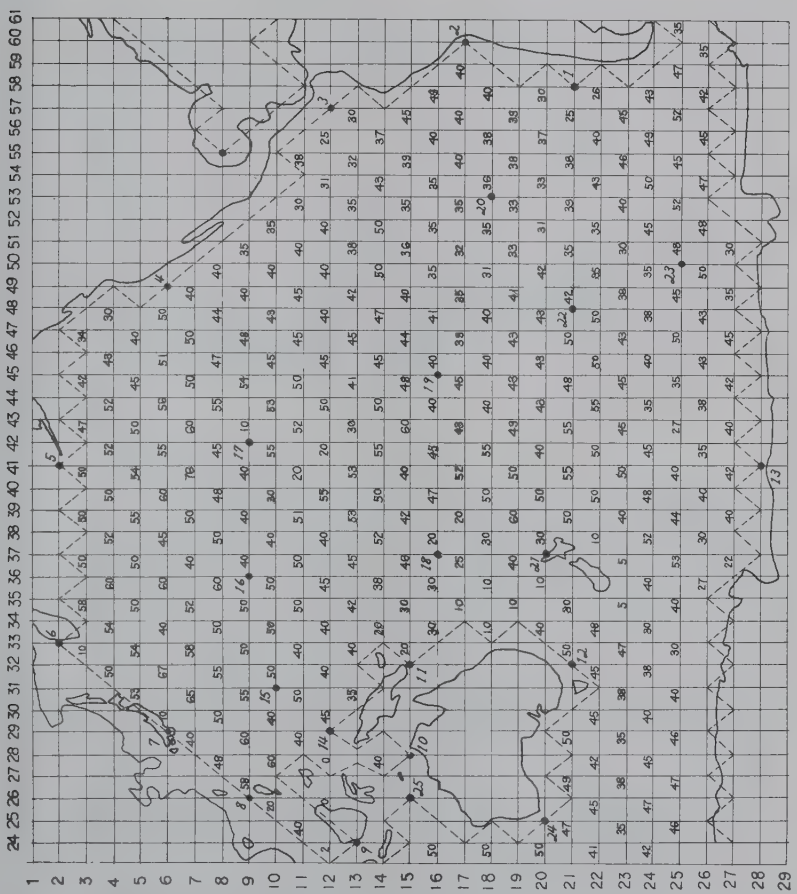

Fig. 3(b). Computed area and depth (100 m. unit). Dots are representative stations.

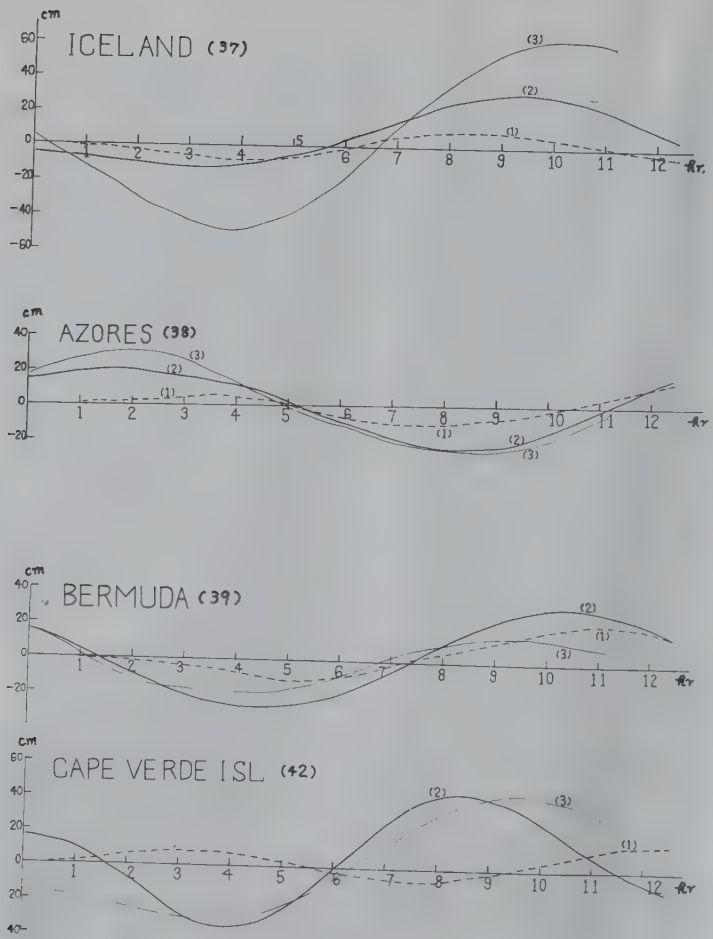

Fig. 4(a). The variation of M_2 elevation. Numbers correspond to Fig. 3.

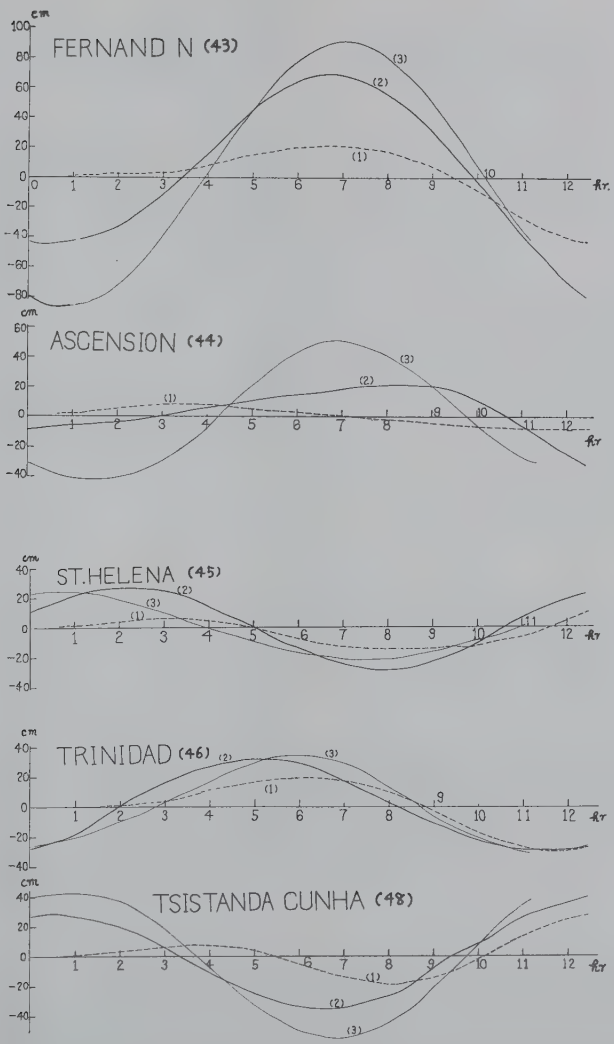

Fig. 4(b). The variation of M_2 elevation. Numbers correspond to Fig. 3.

The Oceanographical Magazine
Vol. 15. No. 2, January 1964

An Observation of a Deep Current in the Southern East Sea of Tori Shima*

By

Tosio NAN'NITI — *Meteorological Research Institute, Tokyo*
Hideo AKAMATSU — *Japan Meteorological Agency*
Toshisuke NAKAI — *Japan Meteorologicrl Agency*
Kazutoshi FUJII — *Japan Meteorological Agency*

Abstract: A 5-day series of measurements of deep current with a neutrally-buoyant float at 1000 m depth was made at 30°N at a distance of 143 km from Tori Shima. The mean of the current measurements was 3 cm/sec toward 244° true, and it exhibited a significant oscillation of about 24-hr period. This direct measurement of current shows that there is the southwest-ward flowing water actross the Ogasawara submarine ridge and vice versa.

1. Introduction

It is said that the sea conditions of the north west Pacific near Japan are divided into two regions by the Izu (or Ogasawara) submarine ridge. The aim of the work described here was to study the exchange of water between them across the submarine ridge, especially to ascertain the orign of the intermediate water which is considered to maintain the cold water region of Enshū-Nada Sea (NAN'NITI 1960, 1962).

The choice of area was controlled by several factors. A fairly flat and deep sea-floor across the submarine ridge seemed desirable, so that the deep water can flow well across the ridge. The neighbourhood of 29°47′N, 141°41′E seemed most suitable (Fig. 1). It is the deepest basin across the ridge between Tori Shima and Bonin Islands, and is near the Ramapo Deep.

2. Methods of measuring currents

In tracking a neutrally-buoyant float, an accuracy of the measurement is limitted by uncertainties in fixing the ship's position. The area chosen for the present measurements was within the ground-wave coverage of Loran stations 2H5 and 2H6, the accuracy in good fixes on the R. S. Ryofu Maru is about ±0.5 miles, sometimes ±1.0 miles.

* JEDS Contribution No. 53

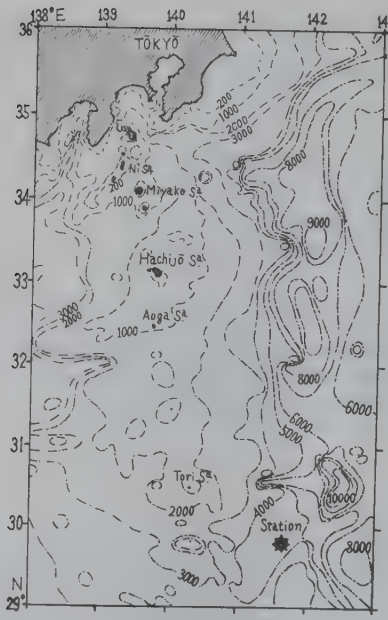

Fig. 1. Locality chart.

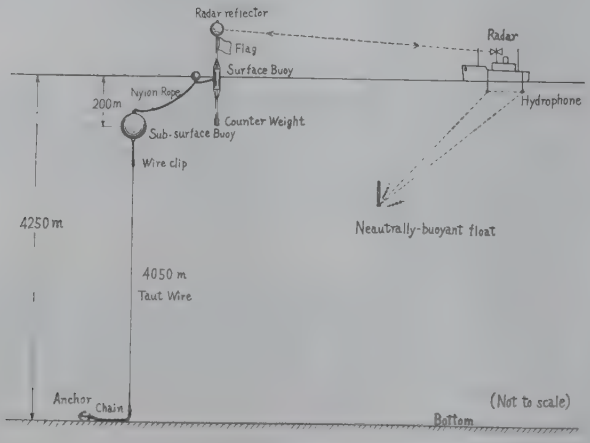

Fig. 2. Schematic figure of obervation.

Anchor and Chain

Surface Buoy.

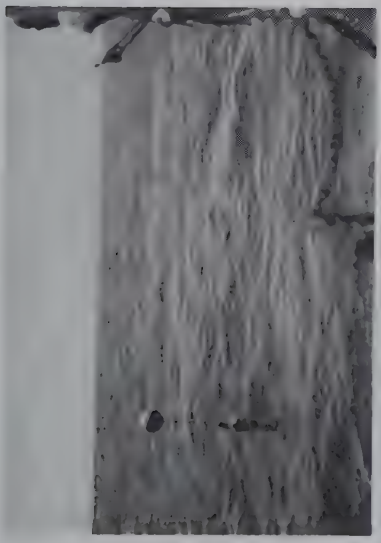

Surface-Buoy.

Sub-surface Buoy.

To keep the fixing of the ship's position in a good accuracy by radar fixes on an anchored buoy, we searched a fairly flat sea-floor by precisely echo sounding, and found the area to be the station, the depth of which showed 4200± 100 m with a radius of 5 miles. At this position, we set an anchored buoy such as shown in Fig. 2, the depth is about 4250 m.

Starting at the bottom, the buoy system used on Ryofu Maru consisted of a 80 kg anchor, a 155 kg chain, a mooring wire about 4050 m long (No. 19, 3 mm diameter, weight 44 kg/1000 m, 880 kg breaking strength) attached to a underwater buoy, 100 cm steel sphere (weight 496 kg, positive buoyancy 276 kg). The length of mooring wire predetermined to keep the underwater buoy about 200 m below the surface. Five hundred meters of 12 mm diameter nylon cross rope (1200 kg breaking strength) ran from the underwater buoy to the surface buoy (a 70 cm diameter, 100 cm long, steel cylinder), with a counter weight of 50 kg at the bottom, a light and radar reflector at the top 3 m above the sea surface.

One could determine the ship's position with great accuracy by radar from the anchored buoy within a radius of 8 miles.

(1). Accuracy of ship's position

As shown in Fig. 3, the observation was done within a radius of 6 miles of

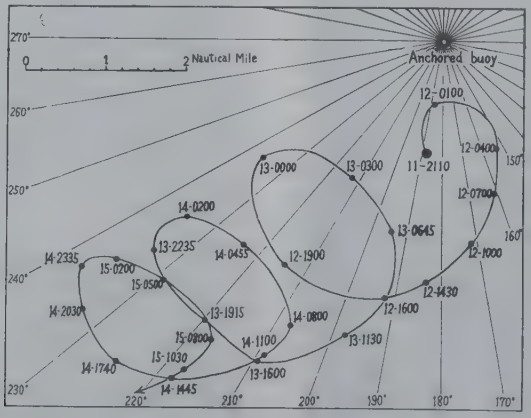

Fig. 3. Track of float. Each dot represents a three-bearing "fix" whose circle of error is generally less than 100 m, the date and time of each fixis indicated.

the anchored buoy. To determine the ship's position, radar fixes from the anchored buoy were taken.

Fluctuation of the buoy's position, freedom of yawing, or the relative yawing to the ship's position, was estimated to be less than 0.06 miles; for wind and sea were moderate throughout the work, the wind was 5～6 m/sec toward NE, the surface current changed only 15° in its direction, and no change in its speed.

Errors of radar fixing are less than 2 % in distance and less than 1° in direction, so the maxinum total error of determination of ship's position is less than 0.18 miles.

(2). *Accuracy of bearing of float*

Bearings of float could be obtained on the acoustic transmitter by stopping the ship head-to-wind and by putting four hydrophones over the both sides, each 30 m apart (NAN'NITI et. al. 1962). It could be estimated with an accuracy of about 0.05 miles. For three or more bearings were taken in quick succession from different positions. Their intersection defining the position of the float in a horizontal plane, in most cace, the bearings intersected well for the position of the float to be determined relative to the ship with an error of less than 0.1 miles, usually about 0.05 miles.

So the absolute position of the float to the anchored buoy could be generally determined with an error of less than 0.23 miles (0.4 km).

3. Observations

During 11th～15th July 1963, a float was used in making the current measurement, loaded for 1000 m depth. The float was tracked for $85^{h}20^{m}$, its track is shown in Fig. 3. The abyssal plain had a mean depth of 4200 m. This deep crosses the Ogasawara ridge (Fig 1) and the general flow of 1000 m layer crossed the ridge at about 3 cm/sec.

The observed track showed a significant oscillation of about 24-hr period. Though KNAUSS (1962) already followed neutrally-buoyant floats set at various depths from 700～3900 m, it is interested to note that an unambiguous internal oscillation was traced with a float at 1000 m depth. The motion observed is not simply an expression of tidal movement. The speeds are several times those expected for open ocean tides. The measurement was made at about 30° latitude, where resonance of the diurnal tide with the inertia period might occour (J. L. REID Jr. 1962). Or there might be another disturbance which was caused by irregularities in bottom topography.

4. Results

The float exhibited a marked periodic motion and moved in a clockwise orbit at speeds of 12.0~17.5 cm/sec and with a period of approximately 24 hours. The orbital speed is several times that of the translational velocity (3 cm/sec).

The translational component is obtained at 3 cm/sec toward 244° true using a least squre method. After the translational component has been removed, east-west and north-south components of movement plotted against time are shown in Fig. 4, and the orbital motion is shown in Fig. 5. Its orbit had slightly

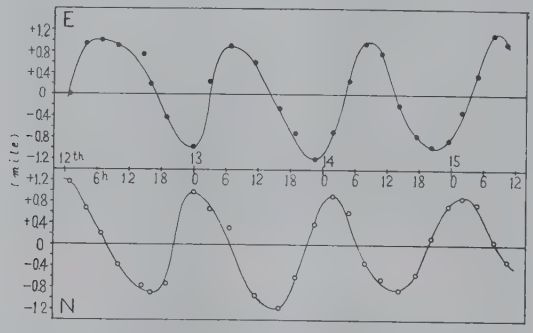

Fig. 4. East-west and north-south components of movement plotted against time. The unit of the ordinate axis is nautical mile; time is plotted along the abscissa.

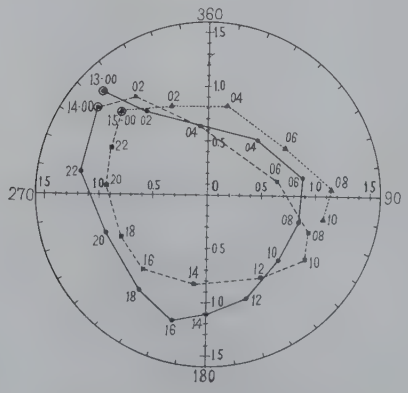

Fig. 5. Orbital motion of float. The unit of co-ordinates is nautical mile.

decreased in its size, the result of the harmonic analysis may be written

$$\text{N—Component}=0.877\cos(\sigma t-14^\circ),$$
$$\text{E—Component}=0.977\cos(\sigma t-133^\circ).$$

The dimension of the elliptical orbit is 2.3 miles of the major axis and 1.3 miles of the minor one respectively, and the mean speed of orbital motion is about 12 cm/sec. The half-pendulum day at 29°44′ latitude, the mean location of observation, is 24.2 hr, and its diameter of the circular motion is about 1.8 miles as its speed is 11.7 cm/sec. They shows fairly good agreemedt with the observed results.

Furthermore, by the past data of tidal observations at Torishima Island, the tidal period was about 12^h50^m, semi-diurnal tidal period, so the observed float motion was caused by the inertia motion not by the tidal motion.

If the x-axis is taken in the direction of the pressure gradient ($\partial p/\partial y=0$), and this pressure gradient corresponds to a steady current (geostrophic current), then (DEFANT. 1961)

$$U=v_0\sin ft+u_0\cos ft,$$
$$V=v_0\cos ft+u_0\sin ft+V_0,$$

where V_0 is the geostrophic steady current, and $\sqrt{u_0^2+v_0^2}$ is the impulse of disturbance imparted to V_0 at the time $t=0$. If this disturbance is only applied in the direction of the steady current (y-direction) and if at the time $t=0$ the total velocity is denoted by V, then

$$u=(V-V_0)\sin ft \quad \text{and} \quad v=V_0+(V-V_0)\cos ft,$$

or

$$x=\frac{V-V_0}{f}(1-\cos ft) \quad \text{and} \quad y=V_0t-\frac{V-V_0}{f}\sin ft.$$

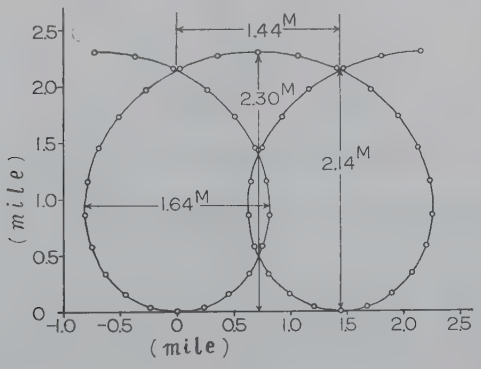

Fig. 6. Track of float theoretically calculated.

Putting observed value $V=0.36$ kt, $V_0=0.06$ kt, $\varphi=30°$, then

$$x=-1.15\cos 15\cdot t+1.15 \quad \text{and} \quad y=-1.15\sin 15\cdot t+0.06t$$

in miles. The result of numerical calculation is shown Fig. 6.

5. Estimating of the depth of a float

Three or more bearings were taken from different ship's positions to decide a float's position in horizontal plane assuming the constant depth of the float to be 1000 m. Conversely, the scattering of bearings could estimate the depth of float to be about 1000±300 m assuming the definite distance in horizontal plane between the ship and the float.

By another method, the expected depth which the float was made neutrally-buoyant was obtained to be 1080 m from observations of temperature and salinity.

6. The method of computing the velocity profiles and volume transport

At four hydrographic stations **A**, **B**, **C**, **D**, bracketing the anchored buoy, temperatures and salinities were observed (Fig. 7). Using the direct-observed velocity

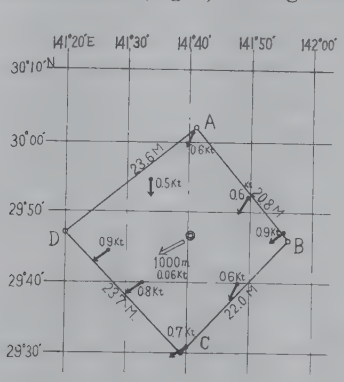

Fig. 7. Hydrographic stations bracketing the anchored buoy.

as a reference, the velocities of 1100 m depth between the pairs of stations $\widehat{AB}$ also $\widehat{CD}$ must be 3 cm/sec and they may be expected to be almost zero between $\widehat{AD}$ also $\widehat{BC}$ assuming that the direct-observed velocity remained unchanged in the vicinity of the anchored station. On the basis of this measurement, the zero velocity line could be determined. Fig. 8 shows the geostrophic currents in each station calculated from each pair of stations. The surface current observations

with the GEK are shown in Fig. 7, they are about 2 or 3 times the geostrophic calculations.

The volume transports were computed simply according to *Area*×*Velocity*. They were obtained as follows.

Section	Volume transport ($\times 10^6 m^3/sec$)	
AB	+0.94	−0.72
BC	+2.56	−0
DA	+2.37	−0
Total	+5.87	−0.72
CD	−5.31	+0

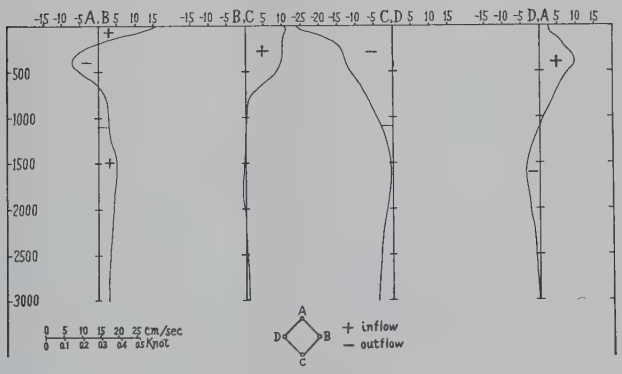

Fig. 8. Geostrophic currents in each section.

They shows that the income volume transport through the sections $\widehat{AB}$, $\widehat{BC}$, $\widehat{DA}$ is approximately same to the outgoing volume transport through the section $\widehat{CD}$. We can have a conclusion that there were the south-west-ward flowing water from the surface to about 1000～1500 meter level, and the north-east-ward undercurrent below this to about 2000 m level. Under this flow, there was again the south-west one to the sea bottom.

To ascertain the orign of the cold water of Enshū-Nada Sea, more observations shall be done.

Acknowledgement: The authors are particularly grateful for the cooperation of members of observation and the crew on board the R. S. Ryofu Maru. Thanks are due also to Mr. M. Yasui for valuable suggestion.

Reference

DEFANT A. (1961): Physical Oceanography. Volume 1. Pergamon Press.

KNAUSS J. A. (1962): Observations of internal waves of tidal period made with neutrally buoyant floats. *Jurn. Mar. Res.*, **20**, 111–118.

NAN'NITI T. (1960): Long-period fluctuations in the Kuroshio. *Pap. Met. Geophyr.*, **11**, 339–347.

—— (1962): A study of the temperature of the surface layer in the Pacific Ocean near Japan. *Pap. Met. Geophys.*, **13**, 196–205.

—— A. WATANABA, H. AKAMATSU and T. NAKAI (1963): Deep current measurements in the cold water mass and vicinity, the Enshū-Nada Sea. *Oceanogr. Mag.*, **14**, 135–139.

REID J. L. Jr. (1962): Observations of inertial rotation and internal waves. *Deep-Sea Res.*, **9**, 283–259.

The Oceanographical Magazine
Vol. 15. No. 2, January 1964

Preliminary Report of the Japanese Expedition of Deep-Sea, the Sixth Cruise, 1963 (JEDS-6)*

By

Hideo Akamatsu

Japan Meteorological Agency

(Received Dec. 17, 1963)

1. *Introduction*

The Japanese Expedition of Deep-Sea, the Sixth Cruise (JEDS-6) which was planned by the Deep-Sea Research Committee (Chairman, K. Wadati), Japan Society for Promotion of Science, was carried out in May, 7 to 29 and in June, 2 to 22, 1963 on board the R/S Ryofu Maru (Captain, T. Suenaga) of the Japan Meteorological Agency. The research stations were occupied at the neighbourhood of the saddle part between the northern part of the Japan Trench and the southwestern part of the Kurile Trench. In the former period, the project aimed mainly to hydrographical researches of the deep-current pattern along the trenches in the area, and a few samplings of bottom sediment, chemical, geophysical, geological observations and so on were also carried out. In the later period, various kinds of geophysical, geological, chemical and biological observation or sampling were carried out. The location of stations is summarized in Fig. 1.

2. *The research members on board the Ryofu Maru*

May 7–29

Japan Meteorological Agency: M. Yasui (Geophys.), H. Akamatsu (Phys. Ocean.), T. Sawara (Phys. Ocean.), T. Nakai (Phys. Ocean.), I. Fujiwara (Phys. Ocean.), T. Akiyama (Chemistry), T. Yura (Chemistry)

Meteorological Research Institute: Y. Sugiura (Chemistry)

Maizuru Marine Observatory: K. Yamamoto (Chemistry)

Nagasaki Marine Observatory: Y. Maeda (Chemistry)

* JEDS Contribution No. 54.

Hydrographic Office: T. SATO (Geology)
Tokyo University: S. UYEDA (Geophys.), J. SEGAWA (Geophys.) M. NOGAMI (Geology)
Hokkaido University: J. ISHII (Geology), A. SHIOZAWA (Geology)
Hokkaido University of Education: K. OSHITE (Geology)

June 2-22

Japan Meteorological Agency: M. YASUI (Geophys.), H. AKAMATSU (Phys. Ocean.), I. FUJIWARA (Maritime Meteor.), T. YURA (Chemistry), Y. KAWARADA (Plankton), K. FURUHASHI (Plankton)
Meteorological Research Institute: Y. SUGIMURA (Chemistry)
Maizuru Marine Observatory: K. HARAMI (Maritime Meteor.)
Tokyo University: J. SEGAWA (Geophys.), H. KAGAMI (Geology)
Hokkaido University: T. MINODA (Plankton)
Tohoku University: M. KOIZUMI (Geology)
Kyoto University: E. HARADA (Benthos), T. NARITA (Benthos)
Shizuoka University: H. MI'I (Geology)
Physical & Chemical Research Institute: S. WATANABE (Phys. Ocean.), M. OKAZAKI (Phys. Ocean.)

3. The items of observation or sampling

(1) Hydrographic cast from surface to bottom:
16 stations (St. 1826–1841)
(2) Water sampling for special chemical analyses:
1828, 1831, 1836, 1839, G 204, G201
(3) Measurements of geothermal gradient:
1826 (G_1), 1837 (G_{12}), G 17, G 202, G 206
(4) Bottom-core sampling:
G 202, G 206, G 207, G 208
(5) Sampling of deep-water plankton:
G 204, G 207
(6) Sampling of benthos and geological material by Beam Trawl:
G 201, G 202, G 203, G 206, G 207
(7) Measurements of Bottom Current:
G 202, G 203, G 206

Besides, the surface current measurements with G. E. K., BT observation, echo sounding and geomagnetic measurement were carried out underway.

Details of results in each branch shall be published in near future by other members and shall be collected in the "Report of JEDS" published by Deep-Sea Research Committee, Japan Society for Promotion of Science.

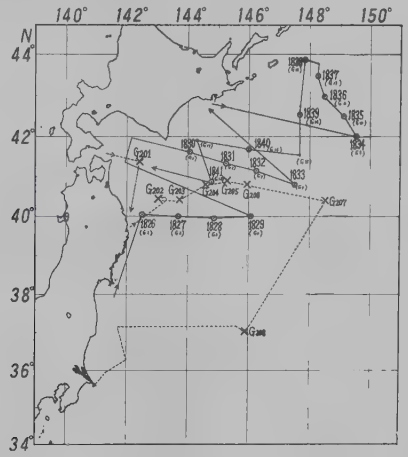

Fig. 1. The observational stations occupied by the Ryofu Maru in the Japanese Expedition of Deep-Sea, the Sixth Cruise (JEDS-6) in May to June, 1963.
--⊙--: Observational line in the former period
--×--: Observational line in the later period

気 象 庁

欧文海洋報告

第 15 巻

THE OCEANOGRAPHICAL MAGAZINE

Vol. 15

Published by the Japan Meteorological Agency

1963 — 1964

CONTENTS

Y. SUGIURA, Y. SUGIMURA, H. YOSHIMURA and T. SHIMANO: Preparation of a stable, dilute solution of phosphate standard for routine work aboard the ship 1

Y. SUGIURA and T. AKIYAMA: Stability of a recording photometer for photometric work aboard the observation ship..... 7

S. MORIYASU: The fluctuation of hydrographic cinditions in the sea south of Honshū, Japan (Review)..... 11

T. UENO and M. MIYAZAKI: Theoretical investigations of typhoon surges along the Japanese coast (III) 31

M. KITOU: On Chaetognaths collected in the Japan Trench-1. The fourth cruise of Japanese Expedition of Deep Sea..... 63

Y. SUGIURA: Time and space variation of the T-Cl relation in Tokyo Bay... 67

M. YASUI, T. UMEZAKI and S. SATO: Short note on the operational breadth of level-winders of hydrographical winches..... 81

T. SAWARA: A short note on nomography for unprotected reversing thermometer..... 85

T. NAKAI: An attempt of slope corrections on echogram in deep-sea..... 89

T. UENO: Theoretical studies on tidal waves travelling over the rotating globe 99

T. NAN'NITI, H. AKAMATSU, T. NAKAI and K. FUJII: An observation of a deep current in the southern east sea of Tori shima 113

H. AKAMATSU: Preliminary report of the Japanese Expedition of Deep-Sea, the sixth cruise, 1963 (JEDS-6) 123

昭和39年3月5日印刷
昭和39年3月10日発行

編集兼発行人　気象庁
東京都千代田区大手町一ノ七

印刷者　花崎実
東京都中央区新富町二ノ十九

印刷所　大東印刷工芸株式会社
東京都中央区新富町二ノ十九